Nonequilibrium molecular conformations in polymer self-consistent field theory

Journal:	*Macromolecules*
Manuscript ID	ma-2020-02002f.R1
Manuscript Type:	Article
Date Submitted by the Author:	27-Oct-2020
Complete List of Authors:	Mueller, Marcus; Georg-August-Universitat Gottingen, Institut fuer Theoretische Physik; Sollich, Peter; Georg-August-Universitat Gottingen, Institut fuer Theoretische Physik Sun, De-Wen; Chang Chun Institute of Applied Chemistry Chinese Academy of Sciences, State Key Laboratory of Polymer Physics and Chemistry

Nonequilibrium molecular conformations in polymer self-consistent field theory

Marcus Müller,*,† Peter Sollich,†,‡ and De-Wen Sun¶

†*Institute for Theoretical Physics, Georg-August-University, 37077 Göttingen, Germany*

‡*King's College London, Department of Mathematics, Strand, London WC2R 2LS, UK*

¶*State Key Laboratory of Polymer Physics and Chemistry, Changchun Institute of Applied Chemistry, Chinese Academy of Sciences, Changchun 130022, P. R. China*

E-mail: mmueller@theorie.physik.uni-goettingen.de

Abstract

The morphology of a multicomponent polymer melt within Self-Consistent Field Theory (SCFT) is completely characterized by the spatial density distribution of the components. SCFT therefore assumes that the molecular conformations are fast variables that adopt their equilibrium statistics with respect to a given density distribution. There are multiple situations – *e.g.*, the early stages of structure formation – where this assumption breaks down because the densities evolve significantly on the time scale of the single-chain relaxation. Here we develop a SCFT that uses as slow variables both, densities and the variance of the first, most slowly relaxing Rouse mode, and design a numerical scheme for its solution based on single-chain propagators. Applications to diblock and multiblock copolymers are presented.

Introduction

In the theory of multicomponent polymer melts, the local variation of segment densities is typically employed to provide a faithful characterization of the state of the system in and out of equilibrium.

Self-Consistent Field Theory (SCFT)[1–10] associates with each density distribution a free energy, $\mathcal{F}$, and the concomitant chemical potential is employed, *e.g.*, in Dynamic Self-Consistent Field Theory (D-SCFT)[11–15] or Minimum Free Energy Path (MFEP)-calculations[16–18] to investigate the kinetics of structure formation or the mechanism of morphology transformations, respectively.

By using the free-energy functional of SCFT in nonequilibrium situations, one tacitly assumes that the densities are the *only* slow degrees of freedom, whereas all other characteristics relax on a significantly faster time scale.[19] This separation of time scales, however, breaks down in nonequilibrium processes where the large-scale chain conformations evolve on the same time scale as or even more slowly than the densities. Nonequilibrium molecular conformations may give rise to a significant process-dependence of material properties.[20–22] There are several examples of this: (i) Spinodal phase separation after a quench of a disordered system initially occurs on the scale of the molecules' end-to-end distance, R_e, and proceeds over a time scale comparable to the time, $T_\mathrm{R} = R_\mathrm{e}^2/D$ (with D being the self-diffusion coefficient of a macromolecule), that the molecules require to diffuse the distance R_e. This time, however, scales like the Rouse time, $\tau_\mathrm{R} = T_\mathrm{R}/3\pi^2$, which characterizes the longest relaxation time of the macromolecular conformations. Thus, there is no time-scale separation between the initial structure formation and the relaxation of chain conformations.[13,23] (ii) In the course of processing, a rapid change of thermodynamic state, *e.g.*, pressure quench or mechanical deformation, can transfer an initial equilibrium state to an unstable starting state, from which the relaxation towards a stable or metastable state proceeds.[24,25] In the unstable starting state both the density distribution and the molecular conformations are out of equilibrium. Furthermore the nonequilibrium molecular conformations differ from those that the molecules would relax to if the densities were constrained. (iii) Nonequilibrium molecular conformations also occur in steady extensional or shear flows[26–31] and affect, *e.g.*, concentration fluctuations in blends and copolymer solutions[32,33] or the alignment of block copolymer morphologies.[34–39] (iv) Finally, in multiblock copolymers that form loops and bridges[40–43] between microphase-separated domains, structure formation of the density is faster than the relaxation of the fraction of loops and bridges because the required single-chain dynamics is associated with free-energy barriers that

substantially exceed the thermal energy, $k_{\mathrm{B}}T$.[44] These examples motivate the need for a free energy as a functional of the local densities *and* collective quantities that characterize the slowly relaxing chain conformations.

Which quantity characterizes the slow relaxation of molecular conformations? A single-molecule conformation is completely characterized by the positions, $\{\mathbf{r}(s)\}$, of its segments, where $0 \leq s \leq 1$ denotes the contour variable along the macromolecular backbone. We are looking for a *collective* quantity that characterizes the slowly relaxing, large-scale shape of macromolecules. There are several options: (i) From the point of view of rubber elasticity or fluid dynamics, it is natural to characterize the chain conformations by the elastic, single-chain stress or the conjugate strain.[6] Even in the Rouse model[45] for a spatially homogeneous homopolymer melt, however, the stress relaxation is not simple.[46] The stress involves all Rouse modes, and its autocorrelation function decays like a power law in time. Phenomenologically, deformations on all length scales contribute to the stress but the relaxation on the shortest length scale of a bond is faster by a factor N^2 (with N being the number of segments) in the Rouse model than the relaxation of the overall shape, as quantified, *e.g.*, by the second-rank tensor of the end-to-end vector.[27] (ii) From the perspective of polymer dynamics, a focus on quantifying the overall shape of the macromolecule suggests itself. In the context of flowing polymer melts, Mavrantzas and Theodorou used the second-rank tensor of the end-to-end vector[27] as a slow, structural variable, while Ilg, Öttinger, and Kröger employed the mean tensor of gyration.[30] Also models that account for multiple conformation tensors have been devised.[47] In a similar spirit, we choose the mean second-rank tensor, $\mathbb{X}_1^2$, formed by the first Rouse modes, $\hat{\mathbf{X}}_1$. The Rouse modes, $\hat{\mathbf{X}}_p$ with $p = 0, 1, \ldots$ are the normal modes of the Edwards Hamiltonian that describes the unperturbed Gaussian chain conformations

$$\hat{\mathbf{X}}_p[\hat{\mathbf{r}}] \equiv \int_0^1 \mathrm{d}s\, \hat{\mathbf{r}}(s)\, \cos(\pi p s) \qquad \text{and} \qquad \hat{\mathbf{r}}(s) \;=\; \hat{\mathbf{X}}_0 + 2\sum_{p=1}^{\infty} \hat{\mathbf{X}}_p\, \cos(\pi p s) \tag{1}$$

In a spatially homogeneous melt of unentangled homopolymers, the first Rouse mode exhibits a single-exponential decay and the concomitant time scale characterizes the longest relaxation time

of the macromolecular conformations, *i.e.*, it is the slowest structural variable.[45,46] This variable also has a simple behavior under deformation or flow. For instance, a steady state shear flow of a homopolymer melt with rate $\dot{\gamma}_{xy}$ gives rise to[26]

$$\mathbb{X}_1^2 \equiv \langle \hat{\mathbf{X}}_1 \hat{\mathbf{X}}_1^{\mathrm{T}} \rangle = \frac{R_{\mathrm{e}}^2}{6\pi^2} \begin{pmatrix} 1 + \frac{(\dot{\gamma}_{xy}\tau_{\mathrm{R}})^2}{2} & \frac{\dot{\gamma}_{xy}\tau_{\mathrm{R}}}{2} & 0 \\ \frac{\dot{\gamma}_{xy}\tau_{\mathrm{R}}}{2} & 1 & 0 \\ 0 & 0 & 1 \end{pmatrix} + \mathcal{O}\left([\dot{\gamma}_{xy}\tau_{\mathrm{R}}]^3\right) \tag{2}$$

where R_{e} denotes the end-to-end distance of the Gaussian chains in the absence of flow. Moreover, we will show that in lamellae-forming multiblock copolymers, the number of loops and bridges is approximately related to $\mathbb{X}_1^2$ (see below, Equation 114).

Since the second Rouse mode relaxes only a factor of 4 faster than the first one, there is no pronounced time scale separation between the first few Rouse modes.[30] Thus, we consider our approach as a first, systematic step towards incorporating the slowly relaxing polymer conformations, and the theory could be extended further by incorporating additional higher-order Rouse modes as arguments of the free-energy functional.

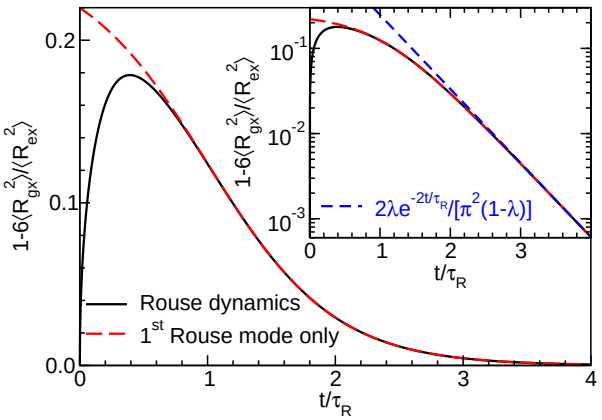

Figure 1: Relaxation of the ratio $1 - 6\langle \hat{R}_{gx}^2 \rangle / \langle \hat{R}_{ex}^2 \rangle$ after an affine stretch with $\lambda = 0.9$. The solid line presents the prediction of the Rouse model according to Equation 3 and Equation 4, whereas the dashed line shows the result when keeping only the relaxation of the first Rouse mode, thus assuming that all higher modes equilibrate instantaneously. The inset highlights the exponential decay at long times, $1 - 6\langle \hat{R}_{gx}^2 \rangle / \langle \hat{R}_{ex}^2 \rangle \approx \frac{2\lambda}{\pi^2(1-\lambda)} \exp\left(-2t/\tau_{\mathrm{R}}\right)$.

To illustrate the effect of scale-dependent relaxation, we consider a homogeneous melt of unentangled Gaussian chains with mean-squared end-to-end distance, $\langle \hat{R}_{ex} \rangle$ along the x direction. At time $t = 0$, the chains are affinely stretched by a factor $\frac{1}{\sqrt{1-\lambda}} > 1$, and we consider the relaxation

of the chain conformations back to their Gaussian equilibrium conformation. Within the Rouse model, the p^{th} Rouse model relaxes exponentially on the time scale τ_{R}/p^2, and we obtain the time dependence of end-to-end distance and radius of gyration along the stretching direction

$$\langle \hat{R}^2_{ex} \rangle = \frac{R^2_{\text{e}}}{3} + \frac{8R^2_{\text{e}}\lambda}{3\pi^2(1-\lambda)} \sum_{\text{odd}\, p} \frac{e^{-2p^2 t/\tau_{\text{R}}}}{p^2} \tag{3}$$

$$\langle \hat{R}^2_{gx} \rangle = \frac{R^2_{\text{e}}}{18} + \frac{R^2_{\text{e}}\lambda}{3\pi^2(1-\lambda)} \sum_{p=1}^{\infty} \frac{e^{-2p^2 t/\tau_{\text{R}}}}{p^2} \tag{4}$$

One hallmark of Gaussian chain conformations is the ratio $6\langle \hat{R}^2_{gx} \rangle / \langle \hat{R}^2_{ex} \rangle$ being unity. In Figure 1 we present the time evolution of this ratio. Clearly, the affinely deformed initial and the equilibrated final conformations are Gaussian but on the time scale τ_{R} there are distinct deviations, *i.e.*, the relaxation from a stretched Gaussian conformation to an equilibrated Gaussian configuration proceeds via nongaussian configurations. These configurations cannot be described by a Gaussian chain model with a time-dependent, anisotropic statistical segment length. Figure 1 also shows the time evolution of this ratio under the assumption that all Rouse modes but the first relax instantaneously. Note that that this description is accurate for $t \gtrsim \tau_{\text{R}}$.

In this manuscript, we derive the free energy for dense, multicomponent polymer melts as functional of the local segment densities and the symmetric, mean, second-rank tensor, $\mathbb{X}^2_1$, formed by the first Rouse modes. Thus the system out of equilibrium is described by ϕ_A and $\mathbb{X}^2_1$ and all other variables are assumed to equilibrate given the constraints on ϕ_A and $\mathbb{X}^2_1$. The values of these constrained quantities have to be worked out for specific nonequilibrium situations –if on the other hand the system did reach full equilibrium, these constraints would be absent. In the following section, we derive the formalism. Then, we describe its efficient, numerical implementation for lamellae-forming diblock and multiblock copolymers, using single-chain propagators in conjunction with a pseudospectral algorithm.[48,49] The subsequent section illustrates the results for two macromolecular architectures, diblock and multiblock copolymers. The manuscript closes with a summary and outlook towards further developments.

Constraining the variance of the first Rouse modes

Model and self-consistent field theory (SCFT)

We consider a dense melt of n copolymers in a volume, V. The copolymer is comprised of two segment species, A and B. Let $\hat{\mathbf{r}}_i(s)$ denote the molecular conformation of polymer $i = 1, \ldots, n$. The hat superscript denotes that a quantity depends on the explicit molecular coordinates. The dimensionless segment density of A segments takes the form

$$\hat{\phi}_A(\mathbf{r}) \equiv \frac{1}{\rho_p} \sum_{i=1}^{n} \int_0^1 \mathrm{d}s \; \gamma_A(s) \delta \left[\mathbf{r} - \hat{\mathbf{r}}_i(s) \right] \tag{5}$$

where $\rho_p = n/V$ denotes the number density of polymers, and $\gamma_A(s) = 1$ if the segment at contour position s is of type A, and zero otherwise. A similar definition holds for the B density. Moreover, we assume incompressibility, *i.e.*, $\hat{\phi}_A(\mathbf{r}) + \hat{\phi}_B(\mathbf{r}) = 1$ at all points in space. Unlike segments repel each other with a strength proportional to χN, where χ denotes the Flory-Huggins parameter and N the number of segments per polymer, respectively.

The variance of the first Rouse modes at position $\mathbf{r}$ is defined by the symmetric, second-rank tensor

$$\hat{\mathbb{X}}_1^2(\mathbf{r}) \;\equiv\; \frac{1}{\rho_p} \sum_{i=1}^{n} \hat{\mathbf{X}}_1[\hat{\mathbf{r}}_i] \hat{\mathbf{X}}_1^{\mathrm{T}}[\hat{\mathbf{r}}_i] \; \delta \left(\mathbf{r} - \mathbf{\Pi}[\hat{\mathbf{r}}_i] \right) \tag{6}$$

where $\mathbf{\Pi}[\hat{\mathbf{r}}_i]$ assigns the conformation of the i^{th} polymer to a position in space. In the following, we will simply assign the variance of the first Rouse mode of a chain to the position of its first segment, *i.e.*, $\mathbf{\Pi}[\hat{\mathbf{r}}_i] = \hat{\mathbf{r}}_i(0)$. Note that the first Rouse mode characterizes the entire macromolecule, and thus alternative assignments of this chain property to a spatial position can be envisioned. The specific form of the assignment will become important if gradients of $\mathbb{X}_1^2(\mathbf{r})$ or its thermodynamically conjugate variable are significant on length scales smaller than R_{e}. In the following, however, we assume that the given variance of the first Rouse modes varies only on length scales that are much larger than R_{e}.

The goal is to compute the free-energy functional, $\mathcal{F}[\phi_A, \mathbb{X}_1^2]$,

$$e^{-\frac{\mathcal{F}[\phi_A,\mathbb{X}_1^2]}{k_\mathrm{B}T}} \equiv \frac{1}{n!}\int \prod_{i=1}^{n} \mathcal{D}[\hat{\mathbf{r}}_i]\mathcal{P}[\hat{\mathbf{r}}_i]\; e^{-\chi N\rho_p \int \mathrm{d}\mathbf{r}\; \hat{\phi}_A\hat{\phi}_B}\delta(\hat{\phi}_A+\hat{\phi}_B-1)\delta(\phi_A-\hat{\phi}_A)\delta(\mathbb{X}_1^2-\hat{\mathbb{X}}_1^2) \tag{7}$$

for a given collective density, ϕ_A, and symmetric variance of first Rouse modes, $\mathbb{X}_1^2$ (within a mean-field approximation). $\mathcal{D}[\mathbf{r}_i]$ sums over all conformations of macromolecule i, and $\mathcal{P}[\hat{\mathbf{r}}_i]$ denotes the Boltzmann weight of the bonded interactions along the Gaussian chain, *i.e.*, $\mathcal{P}[\hat{\mathbf{r}}_i] = e^{-\frac{3}{2R_\mathrm{e}^2}\int_0^1 \mathrm{d}s \left|\frac{\mathrm{d}\hat{\mathbf{r}}_i}{\mathrm{d}s}\right|^2}$. The third and fourth factors represent the nonbonded interactions, giving rise to microphase separation into A- and B-rich domains and a uniform total density, respectively. The last two factors constrain the microscopic density and variance of first Rouse modes that are computed from the polymer configuration, $\{\hat{\mathbf{r}}_i(s)\}$, to the given, slow collective variables, ϕ_A and $\mathbb{X}_1^2$.

In analogy to the well-known procedure of SCFT, we utilize the Fourier representation of the δ-functions,[3,4] introducing integrals over auxiliary fields Ω_A and Ω_B that are conjugate to the segment densities and a symmetric 3×3 matrix $\mathbb{\Lambda}$ – a tensorial orienting field[27,47] – that is thermodynamically conjugate to the symmetric, second-rank tensor $\mathbb{X}_1^2$:

$$\begin{aligned}
e^{-\frac{\mathcal{F}[\phi_A,\mathbb{X}_1^2]}{k_\mathrm{B}T}} &= \frac{1}{n!}\int_{-i\infty}^{i\infty}\mathcal{D}[\Omega_A,\Omega_B,\mathbb{\Lambda}]\int\prod_{i=1}^{n}\mathcal{D}[\hat{\mathbf{r}}_i]\mathcal{P}[\hat{\mathbf{r}}_i]\; e^{-\chi N\rho_p\int\mathrm{d}\mathbf{r}\;\phi_A(1-\phi_A)} \\
&\qquad e^{\rho_p\int\mathrm{d}\mathbf{r}\{\Omega_A(\phi_A-\hat{\phi}_A)+\Omega_B(1-\phi_A-\hat{\phi}_B)-\frac{3\pi^2}{R_\mathrm{e}^2}\mathbb{\Lambda}:(\mathbb{X}_1^2-\hat{\mathbb{X}}_1^2)\}} \qquad (8)\\
&= \int_{-i\infty}^{i\infty}\mathcal{D}[\Omega_A,\Omega_B,\mathbb{\Lambda}]\; e^{-\rho_p\int\mathrm{d}\mathbf{r}\left\{\chi N\phi_A(1-\phi_A)-\Omega_A\phi_A-\Omega_B(1-\phi_A)+\frac{3\pi^2}{R_\mathrm{e}^2}\mathbb{\Lambda}:\mathbb{X}_1^2\right\}} \\
&\qquad \frac{1}{n!}\int\prod_{i=1}^{n}\mathcal{D}[\hat{\mathbf{r}}_i]\mathcal{P}[\hat{\mathbf{r}}_i]\; e^{-\rho_p\int\mathrm{d}\mathbf{r}\{\Omega_A\hat{\phi}_A+\Omega_B\hat{\phi}_B-\frac{3\pi^2}{R_\mathrm{e}^2}\mathbb{\Lambda}:\hat{\mathbb{X}}_1^2\}} \qquad (9)\\
&= \int_{-i\infty}^{i\infty}\mathcal{D}[\Omega_A,\Omega_B,\mathbb{\Lambda}]\;\exp\left(-\frac{\mathscr{F}[\Omega_A,\Omega_B,\mathbb{\Lambda}|\phi_A,\mathbb{X}_1^2]}{k_\mathrm{B}T}\right) \qquad (10)
\end{aligned}$$

with

$$\begin{aligned}
\frac{\mathscr{F}[\Omega_A,\Omega_B,\mathbb{\Lambda}|\phi_A,\mathbb{X}_1^2]}{k_\mathrm{B}T\sqrt{\mathcal{N}}V/R_\mathrm{e}^3} &= \ln\frac{n}{eV\mathcal{Z}_0}-\ln\frac{\mathcal{Q}[\Omega_A,\Omega_B,\mathbb{\Lambda}]}{V\mathcal{Z}_0} \\
&\quad +\int\frac{\mathrm{d}\mathbf{r}}{V}\left\{\chi N\phi_A(1-\phi_A)-\Omega_A\phi_A-\Omega_B(1-\phi_A)+\frac{3\pi^2}{R_\mathrm{e}^2}\mathbb{\Lambda}:\mathbb{X}_1^2\right\} \qquad (11)
\end{aligned}$$

where $\bar{\mathcal{N}} = (\rho_p R_e^3)^2$ is the invariant degree of polymerization, and $\mathcal{Z}_0 \equiv \frac{1}{V}\int \mathcal{D}[\hat{\mathbf{r}}]\mathcal{P}[\hat{\mathbf{r}}]$ denotes the partition function of polymer conformations in the absence of external fields or nonbonded interactions. The functional integral over the symmetric, tensorial orienting field, $\mathbb{\Lambda}(\mathbf{r})$, runs over the 6 independent component fields. Similar tensorial fields are employ in field-theoretic treatments of Maier-Saupe interactions in liquid-crystalline polymers.[50–54] At the saddlepoint of the integral, the auxiliary collective fields Ω_A, Ω_B, and $\mathbb{\Lambda}$ are real such that we recover the canonical-ensemble form within a mean-field approximation (see below). The coefficient $3\pi^2/R_e^2$ has been chosen such that $\mathbb{\Lambda}$ is dimensionless and the eigenvalues of $\mathbb{\Lambda}$ at the saddlepoint of the integral are smaller than 1. [1] $\mathcal{Q}$ denotes the partition function of a single chain subjected to the auxiliary fields, Ω_A, Ω_B, and $\mathbb{\Lambda}$ that couple to the segment densities and variance of the first Rouse modes, respectively:

$$\begin{aligned}
\mathcal{Q}[\Omega_A,\Omega_B,\mathbb{\Lambda}] &= \int \mathcal{D}[\hat{\mathbf{r}}]\mathcal{P}[\hat{\mathbf{r}}]\; e^{-\int_0^1 \mathrm{d}s\,\{\gamma_A(s)\Omega_A(\hat{\mathbf{r}}(s))+[1-\gamma_A(s)]\Omega_B(\hat{\mathbf{r}}(s))\}} \\
&\qquad e^{\frac{3\pi^2}{R_e^2}\sum_{\alpha\beta}\mathbb{\Lambda}_{\alpha\beta}(\mathbf{\Pi}[\hat{\mathbf{r}}])\;\int_0^1 \mathrm{d}s_1\;\int_0^1 \mathrm{d}s_2\;\hat{r}_\alpha(s_1)\hat{r}_\beta(s_2)\;\cos(\pi s_1)\cos(\pi s_2)} \qquad (12)\\
&= \int \mathcal{D}[\hat{\mathbf{r}}]\mathcal{P}[\hat{\mathbf{r}}]\; e^{-\int_0^1 \mathrm{d}s\;\Omega(\hat{\mathbf{r}}(s),s)+\frac{3\pi^2}{R_e^2}\hat{\mathbf{X}}_1^{\mathrm{T}}\mathbb{\Lambda}(\mathbf{\Pi}[\hat{\mathbf{r}}])\hat{\mathbf{X}}_1} \qquad (13)\\
\text{with}\qquad \Omega(\mathbf{r},s) &\equiv \gamma_A(s)\Omega_A(\mathbf{r})+[1-\gamma_A(s)]\Omega_B(\mathbf{r}) \qquad (14)
\end{aligned}$$

The functional integral over the auxiliary fields in Equation 10 is difficult to perform and, like in SCFT for Gaussian chains, we approximate it by its saddlepoint value.[3,4] This approximation is accurate for large values of $\bar{\mathcal{N}}$. The saddlepoint values of the auxiliary fields are denoted by lower-case letters. They depend on ϕ_A and $\mathbb{X}_1^2$ and are implicitly determined by the self-consistent

[1] Since $\int \mathcal{D}[\hat{\mathbf{r}}]\mathcal{P}[\hat{\mathbf{r}}]\; e^{+\frac{3\pi^2}{R_e^2}\hat{\mathbf{X}}_1^{\mathrm{T}}\mathbb{\Lambda}\hat{\mathbf{X}}_1}\cdots = \int \mathrm{d}\mathbf{X}_0\;\mathrm{d}\mathbf{X}_1\; e^{-\frac{3\pi^2}{R_e^2}\mathbf{X}_1^{\mathrm{T}}(\mathbb{1}-\mathbb{\Lambda})\mathbf{X}_1}\prod_{p=2}^{\infty}\int \mathrm{d}\mathbf{X}_p\; e^{-\sum_{p=2}^{\infty}\frac{3\pi^2 p^2}{R_e^2}\mathbf{X}_p^2}\cdots$ (see Equation 92) the symmetric matrix $\mathbb{1}-\mathbb{\Lambda}$ must be positive. Positive eigenvalues of $\mathbb{\Lambda}$ give rise to a larger variance of the first Rouse mode than for a Gaussian chain, *i.e.*, the chains are stretched along this eigendirection. Conversely, negative eigenvalues of $\mathbb{\Lambda}$ characterize eigendirections, along which fluctuations of the first Rouse mode are restrained, *i.e.*, the chain conformations are compressed.

set of equations

$$\phi_A(\mathbf{r}) = -V\frac{\delta}{\delta\omega_A(\mathbf{r})}\ln\mathcal{Q}[\omega_A,\omega_B,\mathbb{\lambda}] \tag{15}$$

$$1-\phi_A(\mathbf{r}) = -V\frac{\delta}{\delta\omega_B(\mathbf{r})}\ln\mathcal{Q}[\omega_A,\omega_B,\mathbb{\lambda}] \tag{16}$$

$$\frac{3\pi^2}{R_\mathrm{e}^2}\mathbb{K}_1^2(\mathbf{r}) = +V\frac{\delta}{\delta\mathbb{\lambda}(\mathbf{r})}\ln\mathcal{Q}[\omega_A,\omega_B,\mathbb{\lambda}] \tag{17}$$

Adding spatially constant values to the interaction fields, ω_A or ω_B, alters neither the saddlepoint equations, Equation 15 and Equation 16, nor the value of the free-energy functional, Equation 11, of the canonical ensemble. Therefore, we additionally impose

$$\int\frac{\mathrm{d}\mathbf{r}}{V}\,\omega_B(\mathbf{r}) = \chi N\bar{\phi}_A = \chi N\int\frac{\mathrm{d}\mathbf{r}}{V}\,\phi_A(\mathbf{r}) \qquad \text{and} \qquad \int\frac{\mathrm{d}\mathbf{r}}{V}\,\omega_A(\mathbf{r}) = \chi N(1-\bar{\phi}_A) \tag{18}$$

Inserting the resulting saddlepoint values into Equation 11, $\mathcal{F}[\phi_A,\mathbb{K}_1^2] \approx \mathscr{F}[\omega_A,\omega_B,\mathbb{\lambda}|\phi_A,\mathbb{K}_1^2]$, we obtain the mean-field approximation of the free-energy functional

$$\begin{aligned}\frac{\mathcal{F}[\phi_A,\mathbb{K}_1^2]}{k_\mathrm{B}T\sqrt{\bar{\mathcal{N}}}V/R_\mathrm{e}^3} \approx\ & \ln\frac{n}{eV\mathcal{Z}_0} + \int\frac{\mathrm{d}\mathbf{r}}{V}\,\chi N\phi_A(1-\phi_A) + \frac{3\pi^2}{R_\mathrm{e}^2}\mathbb{\lambda}[\phi_A,\mathbb{K}_1^2]:\mathbb{K}_1^2 \\ & - \ln\frac{\mathcal{Q}[\omega_A[\phi_A,\mathbb{K}_1^2],\omega_B[\phi_A,\mathbb{K}_1^2],\lambda[\phi_A,\mathbb{K}_1^2]]}{V\mathcal{Z}_0} - \int\frac{\mathrm{d}\mathbf{r}}{V}\,\Big\{\omega_A[\phi_A,\mathbb{K}_1^2]\phi_A + \omega_B[\phi_A,\mathbb{K}_1^2](1-\phi_A)\Big\}\end{aligned} \tag{19}$$

as a function of the slow, collective variables, $\phi_A(\mathbf{r})$ and $\mathbb{K}_1^2(\mathbf{r})$. The different terms correspond to the ideal-gas term, the energy of AB repulsion, the free-energy of constraining the variance of the first Rouse modes, and the conformational entropy of the nongaussian polymers in the spatially modulated morphology.

If we minimize the above free-energy functional with respect to $\mathbb{K}_1^2(\mathbf{r})$, we relax the constraint on the variance of the first Rouse modes. Using Equation 15, 16, and 17, we determine the saddlepoint value of $\mathbb{K}_1^2(\mathbf{r})$ (*i.e.*, the unconstrained, equilibrium value) from

$$\mathbb{\mu}_{\mathbb{K}_1^2} \equiv \frac{R_\mathrm{e}^3}{k_\mathrm{B}T\sqrt{\bar{\mathcal{N}}}}\frac{\delta\mathcal{F}}{\delta\mathbb{K}_1^2(\mathbf{r})} = \frac{3\pi^2}{R_\mathrm{e}^2}\,\mathbb{\lambda} \stackrel{!}{=} 0 \tag{20}$$

i.e., $\mathbb{X}_1^2$ relaxes such that the tensorial orienting field, $\mathbb{\lambda}$, vanishes. Using $\mathbb{\lambda} = 0$ in Equation 11 and Equation 13, we recover the standard free-energy functional of SCFT, as expected.

If we only constrain $\mathbb{X}_1^2$ but allow the density, ϕ_A, to relax, we have to minimize $\mathcal{F}[\phi_A, \mathbb{X}_1^2]$ with respect to ϕ_A. Then, we recover the saddlepoint relation between interaction fields and densities of equilibrium SCFT:

$$\mu_{\phi_A} \equiv \frac{R_{\mathrm{e}}^3}{k_{\mathrm{B}}T\sqrt{\bar{\mathcal{N}}}} \frac{\delta \mathcal{F}}{\delta \phi_A(\mathbf{r})} = \chi N(1 - 2\phi_A(\mathbf{r})) - (\omega_A(\mathbf{r}) - \omega_B(\mathbf{r})) \stackrel{!}{=} 0 \tag{21}$$

Calculating the single-chain partition function, $\mathcal{Q}[\omega_A, \omega_B, \mathbb{\lambda}]$

Introducing the contour-position-dependent, pairwise potential between chain segments,

$$\nu(\mathbf{r}_1, s_1, \mathbf{r}_2, s_2) \equiv -\frac{6\pi^2}{R_{\mathrm{e}}^2}\, \mathbf{r}_1^{\mathrm{T}} \mathbb{\lambda}(\mathbf{\Pi}[\hat{\mathbf{r}}])\mathbf{r}_2\, \cos(\pi s_1)\cos(\pi s_2) \tag{22}$$

we can rewrite the single-chain partition function, Equation 13, in the form

$$\mathcal{Q}[\omega_A, \omega_B, \mathbb{\lambda}] = \int \mathcal{D}[\hat{\mathbf{r}}]\mathcal{P}[\hat{\mathbf{r}}]\; e^{-\int_0^1 \mathrm{d}s\, \omega(\hat{\mathbf{r}}(s),s) - \frac{1}{2}\int_0^1 \mathrm{d}s_1 \int_0^1 \mathrm{d}s_2\, \nu(\hat{\mathbf{r}}(s_1),s_1,\hat{\mathbf{r}}(s_2),s_2)} \tag{23}$$

Whereas the saddlepoint values of the auxiliary fields, ω_A and ω_B, act like external fields on a single chain, the tensorial orienting field, $\mathbb{\lambda}$, creates a pairwise interaction between segments at contour positions s_1 and s_2. This pairwise interaction among segments along the same chain breaks the Markov property of the chain conformations that is commonly exploited to rewrite the problem of a single chain in external fields in terms of a modified diffusion equation for single-chain propagators.[1,3,4]

To overcome this complication, we use a Hubbard-Stratonovich transformation to decouple the pairwise interactions along a chain by an auxiliary variable, $\boldsymbol{\eta}$. We write accordingly

$$\exp\left(\frac{3\pi^2}{R_{\mathrm{e}}^2}\hat{\mathbf{X}}_1^{\mathrm{T}}\mathbb{\lambda}\hat{\mathbf{X}}_1\right) = \int \mathrm{d}\boldsymbol{\eta}\, \frac{e^{-\frac{\boldsymbol{\eta}^{\mathrm{T}}\mathbb{\lambda}^{-1}\boldsymbol{\eta}}{12\pi^2}}}{\sqrt{\det(12\pi^3\mathbb{\lambda})}} \exp\left(\boldsymbol{\eta}^{\mathrm{T}}\frac{\hat{\mathbf{X}}_1}{R_e}\right) \tag{24}$$

This version of the transformation applies if all eigenvalues of the real, symmetric matrix $\mathbb{\lambda}$ are positive. In the limit that an eigenvalue tends to zero, $\lambda_\alpha \to 0$, the first term smoothly converges to $\delta(\eta_\alpha)$, *i.e.*, the integral over η_α collapses, and we obtain the standard SCFT in this eigendirection. If $\mathbb{\lambda}$ has negative eigenvalues, we use, for those eigendirections α that have eigenvalues $\lambda_\alpha < 0$, the analog of Equation 24 with a purely imaginary $\eta_\alpha = i\bar{\eta}_\alpha$:

$$\exp\left(\frac{3\pi^2}{R_{\mathrm{e}}^2}\lambda_\alpha \hat{X}_{1\alpha}^2\right) = \frac{1}{\sqrt{12\pi^3|\lambda_\alpha|}}\int \mathrm{d}\bar{\eta}_\alpha \ \exp\left(-\frac{\bar{\eta}_\alpha^2}{12\pi^2|\lambda_\alpha|} + i\bar{\eta}_\alpha\frac{\hat{\mathbf{X}}_1}{R_e}\right) \tag{25}$$

In the following we assume that all eigenvalues are positive, *i.e.*, the macromolecular conformations are stretched. The expressions for negative eigenvalues can be obtained by formally substituting $\eta_\alpha = i\bar{\eta}_\alpha$, as follows by comparing Equation 24 and Equation 25.

Inserting the Hubbard-Stratonovich transformation into the single-chain partition function, Equation 13, and explicitly using the choice $\mathbf{\Pi}[\hat{\mathbf{r}}] = \hat{\mathbf{r}}(0)$, we obtain

$$\begin{aligned}
\mathcal{Q} &= \int \mathrm{d}\mathbf{r}_0 \int_{\hat{\mathbf{r}}(0)=\mathbf{r}_0} \mathcal{D}[\hat{\mathbf{r}}]\mathcal{P}[\hat{\mathbf{r}}]\ e^{-\int_0^1 \mathrm{d}s\ \omega(\hat{\mathbf{r}}(s),s)} \frac{1}{\sqrt{\det(12\pi^3\mathbb{\lambda}(\mathbf{r}_0))}} \int \mathrm{d}\boldsymbol{\eta}\ e^{-\frac{\boldsymbol{\eta}^{\mathrm{T}}\mathbb{\lambda}^{-1}(\mathbf{r}_0)\boldsymbol{\eta}}{12\pi^2}+\boldsymbol{\eta}^{\mathrm{T}}\frac{\hat{\mathbf{X}}_1}{R_e}} \qquad (26)\\
&= \int \mathrm{d}\mathbf{r}_0 \int \mathrm{d}\boldsymbol{\eta}\ \frac{\exp\left(-\frac{\boldsymbol{\eta}^{\mathrm{T}}\mathbb{\lambda}^{-1}(\mathbf{r}_0)\boldsymbol{\eta}}{(12\pi^2)}\right)}{\sqrt{\det(12\pi^3\mathbb{\lambda}(\mathbf{r}_0))}} \int_{\hat{\mathbf{r}}(0)=\mathbf{r}_0} \mathcal{D}[\hat{\mathbf{r}}]\mathcal{P}[\hat{\mathbf{r}}]\ e^{-\int_0^1 \mathrm{d}s\ \omega(\hat{\mathbf{r}}(s),s)+\boldsymbol{\eta}^{\mathrm{T}}\frac{\hat{\mathbf{X}}_1}{R_e}}\\
&\equiv \int \mathrm{d}\mathbf{r}_0 \int \mathrm{d}\boldsymbol{\eta}\ W(\mathbf{r}_0,\boldsymbol{\eta})\ \mathcal{Q}_{\boldsymbol{\eta}}^{\mathbf{r}_0} \qquad \text{with} \qquad W(\mathbf{r}_0,\boldsymbol{\eta}) \equiv \frac{\exp\left(-\frac{\boldsymbol{\eta}^{\mathrm{T}}\left[\mathbb{\lambda}^{-1}(\mathbf{r}_0)-\mathbb{1}\right]\boldsymbol{\eta}}{12\pi^2}\right)}{\sqrt{\det(12\pi^3\mathbb{\lambda}(\mathbf{r}_0))}} \qquad (27)
\end{aligned}$$

where

$$\begin{aligned}
\mathcal{Q}_{\boldsymbol{\eta}}^{\mathbf{r}_0} &\equiv e^{-\frac{\boldsymbol{\eta}^{\mathrm{T}}\boldsymbol{\eta}}{12\pi^2}} \int_{\hat{\mathbf{r}}(0)=\mathbf{r}_0} \mathcal{D}[\hat{\mathbf{r}}]\ e^{-\frac{3}{2R_{\mathrm{e}}^2}\int_0^1 \mathrm{d}s\ \left|\frac{\mathrm{d}\hat{r}}{\mathrm{d}s}\right|^2} \times \exp\left(-\int_0^1 \mathrm{d}s\ \left[\omega(\hat{\mathbf{r}}(s),s) - \boldsymbol{\eta}^{\mathrm{T}}\frac{\hat{\mathbf{r}}(s)}{R_{\mathrm{e}}}\cos(\pi s)\right]\right) \qquad (28)\\
&= e^{-\frac{\boldsymbol{\eta}^{\mathrm{T}}\boldsymbol{\eta}}{12\pi^2}} \int_{\hat{\mathbf{r}}(0)=\mathbf{r}_0} \mathcal{D}[\hat{\mathbf{r}}]\ e^{-\frac{3}{2R_{\mathrm{e}}^2}\int_0^1 \mathrm{d}s\ \left|\frac{\mathrm{d}\hat{r}}{\mathrm{d}s}\right|^2} \times \exp\left(-\int_0^1 \mathrm{d}s\ \left[\omega(\hat{\mathbf{r}}(s),s) + \frac{\boldsymbol{\eta}^{\mathrm{T}}}{\pi R_{\mathrm{e}}}\frac{\mathrm{d}\hat{\mathbf{r}}(s)}{\mathrm{d}s}\sin(\pi s)\right]\right) \qquad (29)
\end{aligned}$$

denotes the partition function of a single chain, starting at $\hat{\mathbf{r}}(0) = \mathbf{r}_0$ and subjected to a contour-position-dependent, external field. Here we use the minimum-image convention to evaluate the displacement, $\hat{\mathbf{r}}(s)$, with respect to the starting position, $\mathbf{r}_0$, in a periodic system. In the last line

we have used partial integration to indicate that the additional interaction gives rise to a preferred orientation of bond vectors parallel (for $s < 1/2$) or antiparallel (for $s > 1/2$) to $\boldsymbol{\eta}$.

Note that in the case of compression, where at least one eigenvalue, λ_α, of $\mathbb{\lambda}$ is negative, this contour-position-dependent, external field is complex, $\eta_\alpha = i\bar{\eta}_\alpha$, and the propagators are complex-valued functions. The prefactor $e^{-\frac{\boldsymbol{\eta}^{\mathrm{T}}\boldsymbol{\eta}}{12\pi^2}}$ is included in the definition of the single-chain partition function, $\mathcal{Q}^{\mathbf{r}_0}_{\boldsymbol{\eta}}$ and the weight, $W(\mathbf{r}_0, \boldsymbol{\eta})$, so that the former takes the simple form $e^{-\bar{\varepsilon}}$ (with $\bar{\varepsilon} = 2\chi N \bar{\phi}_A \bar{\phi}_B$ being the interaction energy per chain) in a spatially homogeneous system (see below Equation 69) as in SCFT of Gaussian chains. Thus, the weight $W(\mathbf{r}_0, \boldsymbol{\eta})$, which is not normalized, describes the change of the non-interacting single-chain partition function due to the orienting field, $\mathbb{\lambda}$, whereas $\mathcal{Q}^{\mathbf{r}_0}_{\boldsymbol{\eta}}$ quantifies the influence of nonbonded interactions on the oriented chains.

$\mathcal{Q}^{\mathbf{r}_0}_{\boldsymbol{\eta}}$ can be obtained by the standard technique, *i.e.*, one defines two single-chain propagators, $q^{\mathbf{r}_0}_{\eta}(\mathbf{r}, s)$ and $q^{\dagger}_{\boldsymbol{\eta}}(\mathbf{r}, s)$. The first propagator describes the probability of a chain fraction of length s that starts at position $\hat{\mathbf{r}}(s = 0) = \mathbf{r}_0$ and terminates at $\hat{\mathbf{r}}(s) = \mathbf{r}$. The second propagator quantifies the probability of a chain fraction of length $1 - s$ whose terminal end, $s = 1$, is located at an arbitrary position, propagates backwards and reaches $\hat{\mathbf{r}}(s) = \mathbf{r}$. They obey Edwards' modified diffusion equations

$$\frac{\partial q^{\mathbf{r}_0}_{\boldsymbol{\eta}}(\mathbf{r}, s)}{\partial s} = \left(\frac{R_{\mathrm{e}}^2}{6} \triangle - \left[\omega(\mathbf{r}, s) - \boldsymbol{\eta}^{\mathrm{T}} \frac{\mathbf{r}}{R_{\mathrm{e}}} \cos(\pi s) \right] \right) q^{\mathbf{r}_0}_{\boldsymbol{\eta}}(\mathbf{r}, s) \tag{30}$$

$$-\frac{\partial q^{\dagger}_{\boldsymbol{\eta}}(\mathbf{r}, s)}{\partial s} = \left(\frac{R_{\mathrm{e}}^2}{6} \triangle - \left[\omega(\mathbf{r}, s) - \boldsymbol{\eta}^{\mathrm{T}} \frac{\mathbf{r}}{R_{\mathrm{e}}} \cos(\pi s) \right] \right) q^{\dagger}_{\boldsymbol{\eta}}(\mathbf{r}, s) \tag{31}$$

with the contour-position-dependent interaction field

$$\omega(\mathbf{r}, s) \equiv \gamma_A(s)\omega_A(\mathbf{r}) + [1 - \gamma_A(s)]\omega_B(\mathbf{r}) \tag{32}$$

and initial conditions

$$q^{\mathbf{r}_0}_{\boldsymbol{\eta}}(\mathbf{r}, 0) = R_{\mathrm{e}}^3 \delta(\mathbf{r} - \mathbf{r}_0) \qquad \text{and} \qquad q^{\dagger}_{\boldsymbol{\eta}}(\mathbf{r}, 1) = 1 \tag{33}$$

The potential term linear in $\mathbf{r}$ in the propagator equations is awkward as it can become large and is difficult to continue across periodic boundaries. We show next that it can be eliminated by an appropriate rescaling of the propagators. For the forward propagator we write

$$p_{\boldsymbol{\eta}}^{\mathbf{r}_0}(\mathbf{r},s) \;=\; q_{\boldsymbol{\eta}}^{\mathbf{r}_0}(\mathbf{r},s)\exp\left(\mathbf{f}(s)^{\mathrm{T}}\mathbf{r}+g(s)\right) \tag{34}$$

From Equation 30 it follows that this obeys

$$\frac{\partial p_{\boldsymbol{\eta}}^{\mathbf{r}_0}(\mathbf{r},s)}{\partial s} = \left(\frac{R_{\mathrm{e}}^2}{6}\triangle - \left[\omega(\mathbf{r},s)-\boldsymbol{\eta}^{\mathrm{T}}\frac{\mathbf{r}}{R_{\mathrm{e}}}\cos(\pi s)\right] + \mathbf{f}'(s)^{\mathrm{T}}\mathbf{r} + g'(s) + \frac{R_{\mathrm{e}}^2}{6}\mathbf{f}^2(s) - \frac{R_{\mathrm{e}}^2}{3}\mathbf{f}^{\mathrm{T}}\nabla\right) p_{\boldsymbol{\eta}}^{\mathbf{r}_0}(\mathbf{r},s) \tag{35}$$

To eliminate the terms linear in $\mathbf{r}$ and the s-dependent constant we therefore require

$$\boldsymbol{\eta}\frac{\cos(\pi s)}{R_{\mathrm{e}}} + \mathbf{f}'(s) = 0, \qquad g'(s) + \frac{R_{\mathrm{e}}^2}{6}\mathbf{f}^2(s) = 0 \tag{36}$$

Together with the initial condition $\mathbf{f}(0) = g(0) = 0$, which ensures that $p_{\boldsymbol{\eta}}^{\mathbf{r}_0}(\mathbf{r},s)$ has the same initial condition as $q_{\boldsymbol{\eta}}^{\mathbf{r}_0}(\mathbf{r},s)$, this yields

$$\mathbf{f}(s) = -\boldsymbol{\eta}\frac{\sin(\pi s)}{\pi R_{\mathrm{e}}}, \qquad g(s) = -\frac{\boldsymbol{\eta}^{\mathrm{T}}\boldsymbol{\eta}}{4\pi^2}\left[s - \frac{\sin(2\pi s)}{2\pi}\right] \tag{37}$$

This scheme can be generalized to alternate slow variables of the form $\hat{\mathbf{X}}[\hat{\mathbf{r}}] = \int_0^1 \mathrm{d}s\, \hat{\mathbf{r}}(s)w(s)$. For instance, $w(s) = \cos(\pi p s)$ corresponds to the p^{th} Rouse mode or $w(s) = \delta(s-1) - \delta(s)$ represents the end-to-end vector.

The appropriate rescaling for the reverse propagator can be found similarly, with the rescaling factor now fixed to be unity at $s = 1$. In summary we have

$$p_{\boldsymbol{\eta}}^{\mathbf{r}_0}(\mathbf{r},s) \;\equiv\; q_{\boldsymbol{\eta}}^{\mathbf{r}_0}(\mathbf{r},s)\exp\left(-\boldsymbol{\eta}^{\mathrm{T}}\frac{\mathbf{r}}{R_{\mathrm{e}}}\frac{\sin(\pi s)}{\pi} - \frac{\boldsymbol{\eta}^{\mathrm{T}}\boldsymbol{\eta}}{12\pi^2}\left[s - \frac{\sin(2\pi s)}{2\pi}\right]\right) \tag{38}$$

$$p_{\boldsymbol{\eta}}^{\dagger}(\mathbf{r},s) \;\equiv\; q_{\boldsymbol{\eta}}^{\dagger}(\mathbf{r},s)\exp\left(+\boldsymbol{\eta}^{\mathrm{T}}\frac{\mathbf{r}}{R_{\mathrm{e}}}\frac{\sin(\pi s)}{\pi} + \frac{\boldsymbol{\eta}^{\mathrm{T}}\boldsymbol{\eta}}{12\pi^2}\left[s - 1 - \frac{\sin(2\pi s)}{2\pi}\right]\right) \tag{39}$$

Note that

$$p_{\boldsymbol{\eta}}^{\mathbf{r}_0}(\mathbf{r},s)p_{\boldsymbol{\eta}}^{\dagger}(\mathbf{r},s)\exp\left(\frac{\boldsymbol{\eta}^{\mathrm{T}}\boldsymbol{\eta}}{12\pi^2}\right) = q_{\boldsymbol{\eta}}^{\mathbf{r}_0}(\mathbf{r},s)q_{\boldsymbol{\eta}}^{\dagger}(\mathbf{r},s) \tag{40}$$

for all $\mathbf{r}$ and s. The modified diffusion equations for the rescaled propagators take the form

$$\frac{\partial p_{\boldsymbol{\eta}}^{\mathbf{r}_0}(\mathbf{r},s)}{\partial s} = \left[\frac{R_{\mathrm{e}}^2}{6}\triangle + \frac{R_{\mathrm{e}}}{3\pi}\sin(\pi s)\boldsymbol{\eta}^{\mathrm{T}}\nabla - \omega(\mathbf{r},s)\right] p_{\boldsymbol{\eta}}^{\mathbf{r}_0}(\mathbf{r},s) = \mathcal{L}(s)\, p_{\boldsymbol{\eta}}^{\mathbf{r}_0}(\mathbf{r},s) \tag{41}$$

$$-\frac{\partial p_{\boldsymbol{\eta}}^{\dagger}(r,s)}{\partial s} = \left[\frac{R_{\mathrm{e}}^2}{6}\triangle - \frac{R_{\mathrm{e}}}{3\pi}\sin(\pi s)\boldsymbol{\eta}^{\mathrm{T}}\nabla - \omega(\mathbf{r},s)\right] p_{\boldsymbol{\eta}}^{\dagger}(\mathbf{r},s) = \mathcal{L}^{\dagger}(s)\, p_{\boldsymbol{\eta}}^{\dagger}(\mathbf{r},s) \tag{42}$$

with the initial conditions

$$p_{\boldsymbol{\eta}}^{\mathbf{r}_0}(\mathbf{r},0) = R_{\mathrm{e}}^3\delta(\mathbf{r}-\mathbf{r}_0) \qquad \text{and} \qquad p_{\boldsymbol{\eta}}^{\dagger}(\mathbf{r},1) = 1 \tag{43}$$

Comparing to Equation 30, we have managed to eliminate the potential linear in $\mathbf{r}$ in the above modified diffusion equations, as was our aim. Therefore it is not necessary to apply the minimum-image convention in periodic systems and numerical inaccuracies due to large external fields are avoided.

To solve the modified diffusion equations we use a pseudospectral algorithm based on the Trotter decomposition

$$p_{\boldsymbol{\eta}}^{\mathbf{r}_0}(\mathbf{r},s+\delta s) = \exp\left[\int_s^{s+\delta s}\mathrm{d}t\ \mathcal{L}(t)\right] p_{\boldsymbol{\eta}}^{\mathbf{r}_0}(\mathbf{r},s) = e^{\int_s^{s+\delta s}\mathrm{d}t\left(\frac{R_{\mathrm{e}}^2}{6}\triangle + \frac{R_{\mathrm{e}}}{3\pi}\sin(\pi t)\boldsymbol{\eta}^{\mathrm{T}}\nabla - \omega(\mathbf{r},t)\right)} p_{\boldsymbol{\eta}}^{\mathbf{r}_0}(\mathbf{r},s) \tag{44}$$

$$\approx e^{-\frac{\delta s}{2}\frac{\omega(\mathbf{r},s+\delta s)+\omega(\mathbf{r},s)}{2}} \cdot e^{\delta s\frac{R_{\mathrm{e}}^2}{6}\triangle - \frac{R_{\mathrm{e}}}{3\pi^2}\left\{\cos(\pi[s+\delta s])-\cos(\pi s)\right\}\boldsymbol{\eta}^{\mathrm{T}}\nabla} \cdot e^{-\frac{\delta s}{2}\frac{\omega(\mathbf{r},s+\delta s)+\omega(\mathbf{r},s)}{2}} p_{\boldsymbol{\eta}}^{\mathbf{r}_0}(\mathbf{r},s)$$

$$p_{\boldsymbol{\eta}}^{\dagger}(\mathbf{r},s-\delta s) = \exp\left[-\int_s^{s-\delta s}\mathrm{d}t\ \mathcal{L}^{\dagger}(t)\right] p_{\boldsymbol{\eta}}^{\dagger}(\mathbf{r},s) = \exp\left[\int_{s-\delta s}^{s}\mathrm{d}t\ \mathcal{L}^{\dagger}(t)\right] p_{\boldsymbol{\eta}}^{\dagger}(\mathbf{r},s) \tag{45}$$

$$\approx e^{-\frac{\delta s}{2}\frac{\omega(\mathbf{r},s)+\omega(\mathbf{r},s-\delta s)}{2}} \cdot e^{\delta s\frac{R_{\mathrm{e}}^2}{6}\triangle - \frac{R_{\mathrm{e}}}{3\pi^2}\left\{\cos(\pi[s-\delta s])-\cos(\pi s)\right\}\boldsymbol{\eta}^{\mathrm{T}}\nabla} \cdot e^{-\frac{\delta s}{2}\frac{\omega(\mathbf{r},s)+\omega(\mathbf{r},s-\delta s)}{2}} p_{\boldsymbol{\eta}}^{\dagger}(\mathbf{r},s)$$

where the middle factor is evaluated by Fourier transform. The additional term, proportional to $\boldsymbol{\eta}$, corresponds to a contour-position-dependent drift and the propagators are real-valued for positive definite $\mathbb{\lambda}$. Otherwise, if the chains are compressed, the propagators, $p_{\boldsymbol{\eta}}^{\mathbf{r}_0}(\mathbf{r},s)$ and $p_{\boldsymbol{\eta}}^{\dagger}(\mathbf{r},s)$

are complex-valued.

These propagators allow us to compute the partial, single-chain partition function, Equation 28; here the Gaussian factor in $\boldsymbol{\eta}$ that we included in the definition of $\mathcal{Q}_{\boldsymbol{\eta}}^{\mathbf{r}_0}$ is canceled exactly by the corresponding factor in the rescaled propagators, Equation 40:

$$\frac{\mathcal{Q}_{\boldsymbol{\eta}}^{\mathbf{r}_0}}{\mathcal{Z}_0} = \int \frac{\mathrm{d}\mathbf{r}}{R_\mathrm{e}^3}\, p_{\boldsymbol{\eta}}^{\mathbf{r}_0}(\mathbf{r},s) p_{\boldsymbol{\eta}}^\dagger(\mathbf{r},s) \qquad \text{for all } s \tag{46}$$

$$= \int \frac{\mathrm{d}\mathbf{r}}{R_\mathrm{e}^3}\, p_{\boldsymbol{\eta}}^{\mathbf{r}_0}(\mathbf{r},1) = p_{\boldsymbol{\eta}}^\dagger(\mathbf{r}_0,0) \tag{47}$$

Using Equation 27, we obtain the single-chain partition function

$$\frac{\mathcal{Q}}{V\mathcal{Z}_0} = \frac{1}{V}\int \mathrm{d}\mathbf{r}_0 \int \mathrm{d}\boldsymbol{\eta}\; W(\mathbf{r}_0,\boldsymbol{\eta})\; p_{\boldsymbol{\eta}}^\dagger(\mathbf{r}_0,0) \tag{48}$$

The saddlepoint value ϕ_A, given by Equation 15, can be separated into

$$\phi_A(\mathbf{r}) = -\frac{V}{\mathcal{Q}}\frac{\delta\mathcal{Q}}{\delta\omega_A(\mathbf{r})} = -\frac{V}{\mathcal{Q}}\int \mathrm{d}\mathbf{r}_0 \int \mathrm{d}\boldsymbol{\eta}\; W(\mathbf{r}_0,\boldsymbol{\eta})\; \frac{\delta\mathcal{Q}_{\boldsymbol{\eta}}^{\mathbf{r}_0}}{\delta\omega_A(\mathbf{r})} \tag{49}$$

where the latter term is evaluated *via* the single-chain propagators

$$\frac{\delta\mathcal{Q}_{\boldsymbol{\eta}}^{\mathbf{r}_0}}{\delta\omega_A(\mathbf{r})} = \frac{\delta}{\delta\omega_A(\mathbf{r})} e^{-\frac{\boldsymbol{\eta}^\mathrm{T}\boldsymbol{\eta}}{12\pi^2}} \int_{\hat{\mathbf{r}}(0)=\mathbf{r}_0} \mathcal{D}[\hat{\mathbf{r}}]\mathcal{P}[\hat{\mathbf{r}}]\; \exp\left(-\int_0^1 \mathrm{d}s\; \left[\omega(\hat{\mathbf{r}}(s),s) - \boldsymbol{\eta}^\mathrm{T}\frac{\hat{\mathbf{r}}(s)}{R_\mathrm{e}}\cos(\pi s)\right]\right) \tag{50}$$

$$= -\frac{\mathcal{Z}_0}{R_\mathrm{e}^3}\int_0^1 \mathrm{d}s\; \gamma_A(s) q_{\boldsymbol{\eta}}^{\mathbf{r}_0}(\mathbf{r},s) q_{\boldsymbol{\eta}}^\dagger(\mathbf{r},s) e^{-\frac{\boldsymbol{\eta}^\mathrm{T}\boldsymbol{\eta}}{12\pi^2}} = -\frac{\mathcal{Z}_0}{R_\mathrm{e}^3}\int_0^1 \mathrm{d}s\; \gamma_A(s) p_{\boldsymbol{\eta}}^{\mathbf{r}_0}(\mathbf{r},s) p_{\boldsymbol{\eta}}^\dagger(\mathbf{r},s) \tag{51}$$

In summary, we obtain

$$\phi_A(\mathbf{r}) = \frac{V}{R_\mathrm{e}^3}\frac{\int \mathrm{d}\mathbf{r}_0 \int \mathrm{d}\boldsymbol{\eta}\; W(\mathbf{r}_0,\boldsymbol{\eta})\; \int_0^1 \mathrm{d}s\; \gamma_A(s) p_{\boldsymbol{\eta}}^{\mathbf{r}_0}(\mathbf{r},s) p_{\boldsymbol{\eta}}^\dagger(\mathbf{r},s)}{\int \mathrm{d}\mathbf{r}_0 \int \mathrm{d}\boldsymbol{\eta}\; W(\mathbf{r}_0,\boldsymbol{\eta})\; p_{\boldsymbol{\eta}}^\dagger(\mathbf{r}_0,0)} \tag{52}$$

and a similar expression holds for the B density. In particular, Equation 52 yields for the spatial average of the density

$$\bar{\phi}_A \equiv \frac{1}{V}\int \mathrm{d}\mathbf{r}\; \phi_A(\mathbf{r}) = \int_0^1 \mathrm{d}s\; \gamma_A(s) \tag{53}$$

as it should be.

Finally, we use Equation 17 to obtain an implicit relation between the saddlepoint value, $\mathbb{\lambda}$, of the tensorial orienting field and the given variance, $\mathbb{X}_1^2$, of the first Rouse modes

$$\mathbb{X}_1^2(\mathbf{r}) = \frac{R_\mathrm{e}^2}{3\pi^2}\frac{V}{\mathcal{Q}}\frac{\delta}{\delta\mathbb{\lambda}(\mathbf{r})}\int \mathrm{d}\mathbf{r}_0 \int_{\hat{\mathbf{r}}(0)=\mathbf{r}_0} \mathcal{D}[\hat{\mathbf{r}}]\mathcal{P}[\hat{\mathbf{r}}]\; e^{-\int_0^1 \mathrm{d}s\; \omega(\hat{\mathbf{r}}(s),s)+\frac{3\pi^2}{R_\mathrm{e}^2}\mathbb{\lambda}(\mathbf{r}_0):\hat{\mathbf{X}}_1\hat{\mathbf{X}}_1^\mathrm{T}} \tag{54}$$

$$= \frac{V}{\mathcal{Q}}\int_{\hat{\mathbf{r}}(0)=\mathbf{r}} \mathcal{D}[\hat{\mathbf{r}}]\mathcal{P}[\hat{\mathbf{r}}]\; \hat{\mathbf{X}}_1\hat{\mathbf{X}}_1^\mathrm{T}\; e^{-\int_0^1 \mathrm{d}s\; \omega(\hat{\mathbf{r}}(s),s)+\frac{3\pi^2}{R_\mathrm{e}^2}\mathbb{\lambda}(\mathbf{r}):\hat{\mathbf{X}}_1\hat{\mathbf{X}}_1^\mathrm{T}} \tag{55}$$

$$= \frac{V\mathcal{Q}^\mathbf{r}}{\mathcal{Q}}\left\langle \hat{\mathbf{X}}_1\hat{\mathbf{X}}_1^\mathrm{T}\right\rangle_{\hat{\mathbf{r}}(0)=\mathbf{r}} \tag{56}$$

where $\mathcal{Q}^\mathbf{r}$ is the partition function of a single chain that starts at $\mathbf{r}$ and $\langle\cdots\rangle_{\hat{\mathbf{r}}(0)=\mathbf{r}}$ denotes the average over all those single-chain conformations. Thus, the saddlepoint value, $\mathbb{\lambda}(\mathbf{r})$, is determined by the condition that the given $\mathbb{X}_1^2(\mathbf{r})$ coincides with the single-chain average of the variance of the first Rouse modes of chains starting at $\hat{\mathbf{r}}(0)=\mathbf{r}$, weighted by the probability, $V\mathcal{Q}^\mathbf{r}/\mathcal{Q}$, that a chain starts at $\hat{\mathbf{r}}(0)=\mathbf{r}$. This probability and the corresponding partition function, $\mathcal{Q}^\mathbf{r}$, can also be expressed in terms of the rescaled propagator:

$$\phi_0(\mathbf{r}) \equiv \frac{V\mathcal{Q}^\mathbf{r}}{\mathcal{Q}} = \frac{V\int \mathrm{d}\boldsymbol{\eta}\; W(\mathbf{r},\boldsymbol{\eta})\; p_{\boldsymbol{\eta}}^\dagger(\mathbf{r},0)}{\int \mathrm{d}\mathbf{r}_0 \int \mathrm{d}\boldsymbol{\eta}\; W(\mathbf{r}_0,\boldsymbol{\eta})\; p_{\boldsymbol{\eta}}^\dagger(\mathbf{r}_0,0)} \tag{57}$$

In order to evaluate $\mathbb{X}_1^2(\mathbf{r})$ from Equation 56 we also need to compute the single-chain average of the variance of the first Rouse modes. This can be obtained from the generating function, $G^\mathbf{r}$, of the distribution of $\hat{\mathbf{X}}_1$

$$G^\mathbf{r}(\boldsymbol{\sigma}) \equiv \left\langle \exp\left(\boldsymbol{\sigma}^\mathrm{T}\frac{\hat{\mathbf{X}}_1}{R_\mathrm{e}}\right)\right\rangle_{\hat{\mathbf{r}}(0)=\mathbf{r}} = \frac{1}{\mathcal{Q}^\mathbf{r}}\int_{\hat{\mathbf{r}}(0)=\mathbf{r}} \mathcal{D}[\hat{\mathbf{r}}]\mathcal{P}[\hat{\mathbf{r}}]\; e^{-\int_0^1 \mathrm{d}s\; \omega(\hat{\mathbf{r}}(s),s)+\frac{3\pi^2}{R_\mathrm{e}^2}\hat{\mathbf{X}}_1^\mathrm{T}\mathbb{\lambda}(\boldsymbol{\Pi}[\hat{\mathbf{r}}])\hat{\mathbf{X}}_1+\boldsymbol{\sigma}^\mathrm{T}\frac{\hat{\mathbf{X}}_1}{R_\mathrm{e}}} \tag{58}$$

Using the Hubbard-Stratonovich transformation, Equation 24, we obtain

$$G^{\mathrm{r}}(\boldsymbol{\sigma}) = \frac{1}{\mathcal{Q}^{\mathrm{r}}}\int \mathrm{d}\boldsymbol{\eta}\, W(\mathbf{r},\boldsymbol{\eta}) e^{-\frac{\boldsymbol{\eta}^{\mathrm{T}}\boldsymbol{\eta}}{12\pi^2}} \int_{\hat{\mathbf{r}}(0)=\mathbf{r}_0} \mathcal{D}[\hat{\mathbf{r}}]\mathcal{P}[\hat{\mathbf{r}}]\; e^{-\int_0^1 \mathrm{d}s\, \omega(\hat{\mathbf{r}}(s),s)+(\boldsymbol{\eta}+\boldsymbol{\sigma})^{\mathrm{T}}\frac{\hat{\mathbf{X}}_1}{R_{\mathrm{e}}}} \tag{59}$$

$$= \frac{1}{\mathcal{Q}^{\mathrm{r}}}\int \mathrm{d}\boldsymbol{\eta}'\, W(\mathbf{r},\boldsymbol{\eta}'-\boldsymbol{\sigma}) e^{-\frac{(\boldsymbol{\eta}'-\boldsymbol{\sigma})^{\mathrm{T}}(\boldsymbol{\eta}'-\boldsymbol{\sigma})}{12\pi^2}}\; e^{\frac{\boldsymbol{\eta}'^{\mathrm{T}}\boldsymbol{\eta}'}{12\pi^2}}\, \mathcal{Q}^{\mathrm{r}}_{\boldsymbol{\eta}'} \tag{60}$$

$$= \frac{\mathcal{Z}_0}{\mathcal{Q}^{\mathrm{r}}}\int \mathrm{d}\boldsymbol{\eta}\, W(\mathbf{r},\boldsymbol{\eta}-\boldsymbol{\sigma}) e^{-\frac{\boldsymbol{\sigma}^{\mathrm{T}}\boldsymbol{\sigma}-2\boldsymbol{\eta}^{\mathrm{T}}\boldsymbol{\sigma}}{12\pi^2}}\; p^{\dagger}_{\boldsymbol{\eta}}(\mathbf{r},0) \tag{61}$$

The variance of the distribution is given by

$$\left\langle \hat{\mathbf{X}}_1\hat{\mathbf{X}}_1^{\mathrm{T}}\right\rangle_{\hat{\mathbf{r}}(0)=\mathbf{r}} = R_{\mathrm{e}}^2 \frac{\partial}{\partial\boldsymbol{\sigma}}\frac{\partial}{\partial\boldsymbol{\sigma}}^{\mathrm{T}} G^{\mathrm{r}}(\boldsymbol{\sigma})\Big|_{\boldsymbol{\sigma}=0} \tag{62}$$

$$= R_{\mathrm{e}}^2\frac{\mathcal{Z}_0}{\mathcal{Q}^{\mathrm{r}}}\int \mathrm{d}\boldsymbol{\eta}\; \frac{\partial}{\partial\boldsymbol{\sigma}}\frac{\partial}{\partial\boldsymbol{\sigma}}^{\mathrm{T}} W(\mathbf{r},\boldsymbol{\eta}-\boldsymbol{\sigma}) e^{-\frac{\boldsymbol{\sigma}^{\mathrm{T}}\boldsymbol{\sigma}-2\boldsymbol{\eta}^{\mathrm{T}}\boldsymbol{\sigma}}{12\pi^2}}\Big|_{\boldsymbol{\sigma}=0} p^{\dagger}_{\boldsymbol{\eta}}(\mathbf{r},0) \tag{63}$$

$$= \frac{R_{\mathrm{e}}^2}{6\pi^2}\frac{\mathcal{Z}_0}{\mathcal{Q}^{\mathrm{r}}}\int \mathrm{d}\boldsymbol{\eta}\, W(\mathbf{r},\boldsymbol{\eta})\; \left(\frac{1}{6\pi^2}\mathbb{\lambda}^{-1}(\mathbf{r})\boldsymbol{\eta}\boldsymbol{\eta}^{\mathrm{T}}\mathbb{\lambda}^{-1}(\mathbf{r}) - \mathbb{\lambda}^{-1}(\mathbf{r})\right)\; p^{\dagger}_{\boldsymbol{\eta}}(\mathbf{r},0) \tag{64}$$

$$= \frac{R_{\mathrm{e}}^2}{6\pi^2}\frac{\int \mathrm{d}\boldsymbol{\eta}\, W(\mathbf{r},\boldsymbol{\eta})\; p^{\dagger}_{\boldsymbol{\eta}}(\mathbf{r},0)\;\left(\frac{1}{6\pi^2}\mathbb{\lambda}^{-1}(\mathbf{r})\boldsymbol{\eta}\boldsymbol{\eta}^{\mathrm{T}}\mathbb{\lambda}^{-1}(\mathbf{r}) - \mathbb{\lambda}^{-1}(\mathbf{r})\right)}{\int \mathrm{d}\boldsymbol{\eta}\, W(\mathbf{r},\boldsymbol{\eta})\; p^{\dagger}_{\boldsymbol{\eta}}(\mathbf{r},0)} \tag{65}$$

Instead of adjusting $\mathbb{\lambda}$ according to the saddlepoint condition, Equation 56, we can alternatively consider the tensorial, orienting field, $\mathbb{\lambda}$, as a thermodynamic variable. Since $\mathbb{X}_1^2$ and $\mathbb{\lambda}$ are thermodynamically conjugate variables, we obtain the corresponding free energy, $\mathcal{G}[\phi_A,\mathbb{\lambda}]$ by Legendre transformation

$$\frac{\mathcal{G}[\phi_A,\mathbb{\lambda}]}{k_{\mathrm{B}}T\sqrt{\mathcal{N}}V/R_{\mathrm{e}}^3} \equiv \frac{\mathcal{F}[\phi_A,\mathbb{X}_1^2]}{k_{\mathrm{B}}T\sqrt{\mathcal{N}}V/R_{\mathrm{e}}^3} - \int\frac{\mathrm{d}\mathbf{r}}{V}\,\frac{3\pi^2}{R_{\mathrm{e}}^2}\mathbb{\lambda}:\mathbb{X}_1^2 \tag{66}$$

$$= \ln\frac{n}{eV\mathcal{Z}_0} - \ln\frac{\mathcal{Q}}{V\mathcal{Z}_0} + \int\frac{\mathrm{d}\mathbf{r}}{V}\left\{\chi N\phi_A(1-\phi_A) - \omega_A\phi_A - \omega_B(1-\phi_A)\right\} \tag{67}$$

This free energy per chain is used to determine the lamellar spacing for a given strength of the orienting field, $\mathbb{\lambda}$.

Results

Spatially homogeneous system

It is instructive to consider a spatially homogeneous system, where the slow, collective variables, ϕ_A and $\mathbb{X}_1^2$, do not depend on the position, $\mathbf{r}$, in space. This corresponds, *e.g.*, to a system above the order-disorder transition temperature, $\chi N < \chi_{\mathrm{ODT}} N$, and a homogeneous deformation. Equation 53 yields $\phi_A = \bar{\phi}_A = \int \mathrm{d}s\ \gamma_A(s)$. According to Equation 18 the field can be set to $\omega(\mathbf{r}, s) = \bar{\omega}(s) = \chi N \bar{\phi}_B$ if $\gamma_A(s) = 1$ and $\bar{\omega}(s) = \chi N \bar{\phi}_A$ otherwise. Thus, the interaction energy of a chain in a system with translational invariance is given by $\bar{\varepsilon} = \int_0^1 \mathrm{d}s\ \bar{\omega}(s) = 2\chi N \bar{\phi}_A \bar{\phi}_B$. However, $\mathbb{X}_1^2$ can adopt nontrivial values.

In a homogeneous system, Equation 41 takes the simple form $-\frac{\partial p_{\boldsymbol{\eta}}^\dagger(\mathbf{r},s)}{\partial s} = -\bar{\omega}(s) p_{\boldsymbol{\eta}}^\dagger(\mathbf{r}, s)$, and the initial condition, Equation 43, yields

$$p_{\boldsymbol{\eta}}^\dagger(\mathbf{r}, s) = e^{-\int_s^1 \mathrm{d}s'\ \bar{\omega}(s')} = e^{-\bar{\varepsilon} + \int_0^s \mathrm{d}s'\ \bar{\omega}(s')} \tag{68}$$

Using Equation 47 and Equation 27, we obtain for the single-chain partition function

$$\frac{\mathcal{Q}_{\boldsymbol{\eta}}^{\mathbf{r}_0}}{\mathcal{Z}_0} = p_{\boldsymbol{\eta}}^\dagger(\mathbf{r}_0, 0) = e^{-\bar{\varepsilon}} \tag{69}$$

$$\frac{\mathcal{Q}}{V\mathcal{Z}_0} = \frac{1}{V}\int \mathrm{d}\mathbf{r}_0 \int \mathrm{d}\boldsymbol{\eta}\ \frac{\exp\left(-\frac{\boldsymbol{\eta}^{\mathrm{T}}\left[\mathbb{\lambda}^{-1} - \mathbb{1}\right]\boldsymbol{\eta}}{(12\pi^2)}\right)}{\sqrt{\det(12\pi^3 \mathbb{\lambda})}} e^{-\bar{\varepsilon}} = \frac{e^{-\bar{\varepsilon}}}{\sqrt{\det(\mathbb{1} - \mathbb{\lambda})}} \tag{70}$$

This expression also allows us to explicitly illustrate that, in contrast to integrals over the collective, auxiliary fields, Ω_A, Ω_B, and $\mathbb{\Lambda}$, in Equation 10 for the free energy, the integral over the auxiliary field, $\boldsymbol{\eta}$, in Equation 27 for the single-chain partition function cannot be accurately evaluated by a saddlepoint method because there is no analog of the Ginzburg parameter, $1/\bar{\mathcal{N}}$.

We obtain the variance of the first Rouse modes as a function of $\mathbb{\lambda}$ from Equation 56 and

Equation 65 [2]

$$\mathbb{X}_1^2 = \left\langle \hat{\mathbf{X}}\hat{\mathbf{X}}^{\mathrm{T}} \right\rangle_{\hat{\mathbf{r}}(0)=\mathbf{r}} = \frac{R_{\mathrm{e}}^2}{6\pi^2}\left(\frac{1}{6\pi^2}\mathbb{\lambda}^{-1}\left\{6\pi^2\left[\mathbb{\lambda}^{-1}-\mathbb{1}\right]^{-1}\right\}\mathbb{\lambda}^{-1}-\mathbb{\lambda}^{-1}\right) = \frac{R_{\mathrm{e}}^2}{6\pi^2}\left(\mathbb{1}-\mathbb{\lambda}\right)^{-1} \tag{71}$$

$$\mathbb{\lambda} = \mathbb{1} - \frac{R_{\mathrm{e}}^2}{6\pi^2}\left(\mathbb{X}_1^2\right)^{-1} \tag{72}$$

$\mathbb{\lambda} = 0$ corresponds to the equilibrium of a spatially homogeneous system, where $\mathbb{X}_1^2 = \frac{R_{\mathrm{e}}^2}{6\pi^2}\mathbb{1}$. Inserting these results into Equation 11 and Equation 67, we obtain the free energy per chain in units of $k_{\mathrm{B}}T$ as a function of the given orientational field, $\mathbb{\lambda}$ or the given variance of the first Rouse modes, $\mathbb{X}_1^2$, in a spatially homogeneous system

$$\frac{\mathcal{G}_{\mathrm{hom}}[\mathbb{\lambda}]}{k_{\mathrm{B}}T\sqrt{\mathcal{N}}V/R_{\mathrm{e}}^3} = \ln\frac{n}{eV\mathcal{Z}_0} + \chi N\bar{\phi}_A(1-\bar{\phi}_A) + \frac{1}{2}\ln\det(1-\mathbb{\lambda}) \tag{73}$$

$$\frac{\mathcal{F}_{\mathrm{hom}}[\mathbb{X}_1^2]}{k_{\mathrm{B}}T\sqrt{\mathcal{N}}V/R_{\mathrm{e}}^3} = \ln\frac{n}{eV\mathcal{Z}_0} + \chi N\bar{\phi}_A(1-\bar{\phi}_A) - \frac{1}{2}\ln\det\left(\frac{6\pi^2}{R_{\mathrm{e}}^2}\mathbb{X}_1^2\right) + \frac{1}{2}\mathrm{tr}\left(\frac{6\pi^2}{R_{\mathrm{e}}^2}\mathbb{X}_1^2-1\right) \tag{74}$$

For a system where the first Rouse modes are relaxed, $\mathbb{\lambda} = 0$ and $\mathbb{X}_1^2 = \frac{R_{\mathrm{e}}^2}{6\pi^2}\mathbb{1}$, we recover the standard expression. In the nonequilibrium case, the expression corresponds to previous work using the (first) Rouse mode(s)[55–57], and the second-rank tensor of the end-to-end vector.[27,47]

Additionally, we can compute other conformation properties, *e.g.*, the mean-squared end-to-end distance. In general, the conditional probability, $P^{\mathbf{r}_0}(\mathbf{r},s)$ that a chain that starts at $\mathbf{r}_0$ reaches the position, $\mathbf{r}$, after a contour fraction, s, can be expressed *via* the rescaled propagators

$$P^{\mathbf{r}_0}(\mathbf{r},s) = \frac{1}{R_{\mathrm{e}}^3}\frac{\int \mathrm{d}\boldsymbol{\eta}\, W(\mathbf{r}_0,\boldsymbol{\eta})\, p_{\boldsymbol{\eta}}^{\mathbf{r}_0}(\mathbf{r},s)p_{\boldsymbol{\eta}}^{\dagger}(\mathbf{r},s)}{\int \mathrm{d}\boldsymbol{\eta}\, W(\mathbf{r}_0,\boldsymbol{\eta})\, p_{\boldsymbol{\eta}}^{\dagger}(\mathbf{r}_0,0)} \tag{75}$$

[2]Using Equation 72 in conjunction with Equation 2 to first order in $\dot{\gamma}_{xy}\tau$, we relate the tensorial orienting field $\mathbb{\lambda}$ to the rate-of-strain tensor of a homogeneous, stationary flow,

$$\mathbb{\lambda} = \frac{\dot{\gamma}_{xy}\tau_{\mathrm{R}}}{2}\begin{pmatrix}0&1&0\\1&0&0\\0&0&0\end{pmatrix} + \mathcal{O}\left([\dot{\gamma}_{xy}\tau_{\mathrm{R}}]^2\right)$$

in accord with Ref.[47]

Thus, the spatial profile of the mean-squared end-to-end distance is given by

$$\left\langle \hat{\mathbf{R}}_{\mathrm{e}}^2 \right\rangle_{\hat{\mathbf{r}}(0)=\mathbf{r}_0} = \int \mathrm{d}\mathbf{r}\; P^{\mathbf{r}_0}(\mathbf{r},1)\,[\mathbf{r}-\mathbf{r}_0]^2 = \frac{\int \mathrm{d}\boldsymbol{\eta}\; W(\mathbf{r}_0,\boldsymbol{\eta})\; \int \frac{\mathrm{d}\mathbf{r}}{R_{\mathrm{e}}^3}\; p_{\boldsymbol{\eta}}^{\mathbf{r}_0}(\mathbf{r},1)\,[\mathbf{r}-\mathbf{r}_0]^2}{\int \mathrm{d}\boldsymbol{\eta}\; W(\mathbf{r}_0,\boldsymbol{\eta})\; p_{\boldsymbol{\eta}}^{\dagger}(\mathbf{r}_0,0)} \tag{76}$$

To evaluate this expression for the spatially homogeneous system, we also need the rescaled propagator $p_{\boldsymbol{\eta}}^{\mathbf{r}_0}$. [3]

$$p_{\boldsymbol{\eta}}^{\mathbf{r}_0}(\mathbf{r},s) = \left(\frac{3}{2\pi s}\right)^{3/2} e^{-\int_0^s \mathrm{d}s'\;\bar{\omega}(s')} \exp\left(-\frac{3}{2s}\left[\frac{\mathbf{r}-\mathbf{r}_0}{R_{\mathrm{e}}} - \frac{\boldsymbol{\eta}}{3\pi^2}\left\{\cos(\pi s)-1\right\}\right]^2\right) \tag{77}$$

Using Equation 76 we obtain

$$\left\langle \hat{\mathbf{R}}_{\mathrm{e}}^2 \right\rangle = \frac{\int \mathrm{d}\boldsymbol{\eta}\; W(\mathbf{r}_0,\boldsymbol{\eta})\; \int \frac{\mathrm{d}\mathbf{r}}{R_{\mathrm{e}}^3}\; \frac{\exp\left(-\frac{3}{2}\left[\frac{\mathbf{r}}{R_{\mathrm{e}}}+\frac{2\boldsymbol{\eta}}{3\pi^2}\right]^2\right)}{(2\pi/3)^{3/2}}\mathbf{r}^2}{\int \mathrm{d}\boldsymbol{\eta}\; W(\mathbf{r}_0,\boldsymbol{\eta})} \tag{78}$$

$$= \frac{\int \mathrm{d}\boldsymbol{\eta}\; W(\mathbf{r}_0,\boldsymbol{\eta})\; R_{\mathrm{e}}^2\left(1+\frac{4}{9\pi^4}\boldsymbol{\eta}^{\mathrm{T}}\boldsymbol{\eta}\right)}{\int \mathrm{d}\boldsymbol{\eta}\; W(\mathbf{r}_0,\boldsymbol{\eta})} \tag{79}$$

$$= R_{\mathrm{e}}^2 + \frac{4R_{\mathrm{e}}^2}{9\pi^4}\,\mathrm{tr}\left(6\pi^2\left[\mathbb{\lambda}^{-1}-\mathbb{1}\right]^{-1}\right) = R_{\mathrm{e}}^2 + 16\,\mathrm{tr}\left(\mathbb{X}_1^2 - \frac{R_{\mathrm{e}}^2}{6\pi^2}\mathbb{1}\right) \tag{80}$$

This result agrees with the well-known formula $\left\langle \hat{\mathbf{R}}_{\mathrm{e}}^2 \right\rangle = 16\sum_{\mathrm{odd}\,p}\left\langle \hat{\mathbf{X}}_p^2 \right\rangle = R_{\mathrm{e}}^2 + 16\left(\left\langle \hat{\mathbf{X}}_1^2 \right\rangle - R_{\mathrm{e}}^2\mathbb{1}/[6\pi^2]\right)$.

[3] Using the Fourier transform

$$\tilde{p}_{\boldsymbol{\eta}}^{\mathbf{r}_0}(\mathbf{k},s) \equiv \frac{1}{V}\int \mathrm{d}\mathbf{r}\; p_{\boldsymbol{\eta}}^{\mathbf{r}_0}(\mathbf{r})e^{-i\mathbf{k}^{\mathrm{T}}\mathbf{r}} \qquad \text{and} \qquad p_{\boldsymbol{\eta}}^{\mathbf{r}_0}(\mathbf{r},s) = \sum_{\mathbf{k}} \tilde{p}_{\boldsymbol{\eta}}^{\mathbf{r}_0}(\mathbf{k},s)e^{i\mathbf{k}^{\mathrm{T}}\mathbf{r}}$$

we rewrite Equation 41 in the form

$$\frac{\partial \tilde{p}_{\boldsymbol{\eta}}^{\mathbf{r}_0}(\mathbf{k},s)}{\partial s} = \left[-\frac{\mathbf{k}^{\mathrm{T}}\mathbf{k}R_{\mathrm{e}}^2}{6} + \frac{R_{\mathrm{e}}}{3\pi}\boldsymbol{\eta}^{\mathrm{T}}\sin(\pi s)i\mathbf{k} - \bar{\omega}(s)\right]\tilde{p}_{\boldsymbol{\eta}}^{\mathbf{r}_0}(\mathbf{k},s)$$

This equation has the solution

$$\tilde{p}_{\boldsymbol{\eta}}^{\mathbf{r}_0}(\mathbf{k},s) = \frac{R_{\mathrm{e}}^3}{V}\exp\left(-\int_0^s \mathrm{d}s'\;\bar{\omega}(s') - \frac{\mathbf{k}^{\mathrm{T}}\mathbf{k}R_{\mathrm{e}}^2}{6}s - i\mathbf{k}^{\mathrm{T}}\left[\mathbf{r}_0 + \frac{R_{\mathrm{e}}}{3\pi^2}\boldsymbol{\eta}\left\{\cos(\pi s)-1\right\}\right]\right)$$

that also satisfies the appropriate initial condition.

Lamellar phase of symmetric diblock copolymers

Spatially constant tensorial orienting field $\mathbb{\lambda}$

In the following, we ignore the spatial dependency of the variance of the first Rouse mode, *i.e.*, we do not adjust the saddlepoint value of the auxiliary field, $\mathbb{\lambda}(\mathbf{r})$, so as to fulfill Equation 56 at each point in space. Instead, we assume that $\mathbb{\lambda}$ does not depend on the spatial position. Thus, the weight $W(\mathbf{r},\boldsymbol{\eta})$ is also independent of $\mathbf{r}$, and the saddlepoint condition, Equation 56, and Equation 65 are replaced by

$$\mathbb{\chi}_1^2 = \left\langle \hat{\mathbf{X}}_1 \hat{\mathbf{X}}_1^{\mathrm{T}} \right\rangle \tag{81}$$

$$= \frac{1}{V}\int \mathrm{d}\mathbf{r}\; \phi_0(\mathbf{r})\; \frac{R_\mathrm{e}^2}{6\pi^2}\; \frac{\int \mathrm{d}\boldsymbol{\eta}\; W(\boldsymbol{\eta})\; \left(\frac{1}{6\pi^2}\mathbb{\lambda}^{-1}\boldsymbol{\eta}\boldsymbol{\eta}^{\mathrm{T}}\mathbb{\lambda}^{-1} - \mathbb{\lambda}^{-1}\right)\; p_{\boldsymbol{\eta}}^{\dagger}(\mathbf{r},0)}{\int \mathrm{d}\boldsymbol{\eta}\; W(\boldsymbol{\eta})\; p_{\boldsymbol{\eta}}^{\dagger}(\mathbf{r},0)} \tag{82}$$

$$= \frac{R_\mathrm{e}^2}{6\pi^2}\frac{\int \mathrm{d}\boldsymbol{\eta}\; W(\boldsymbol{\eta}) \int \frac{\mathrm{d}\mathbf{r}}{R_\mathrm{e}^3}\; p_{\boldsymbol{\eta}}^{\dagger}(\mathbf{r},0)\; \left(\frac{1}{6\pi^2}\mathbb{\lambda}^{-1}\boldsymbol{\eta}\boldsymbol{\eta}^{\mathrm{T}}\mathbb{\lambda}^{-1} - \mathbb{\lambda}^{-1}\right)}{\int \mathrm{d}\boldsymbol{\eta}\; W(\boldsymbol{\eta}) \int \frac{\mathrm{d}\mathbf{r}}{R_\mathrm{e}^3}\; p_{\boldsymbol{\eta}}^{\dagger}(\mathbf{r},0)} \tag{83}$$

$$= \frac{R_\mathrm{e}^2}{6\pi^2}\frac{\int \mathrm{d}\boldsymbol{\eta}\; W(\boldsymbol{\eta})\mathcal{Q}_{\boldsymbol{\eta}}\; \left(\frac{1}{6\pi^2}\mathbb{\lambda}^{-1}\boldsymbol{\eta}\boldsymbol{\eta}^{\mathrm{T}}\mathbb{\lambda}^{-1} - \mathbb{\lambda}^{-1}\right)}{\int \mathrm{d}\boldsymbol{\eta}\; W(\boldsymbol{\eta})\mathcal{Q}_{\boldsymbol{\eta}}} \qquad \text{with} \qquad \frac{\mathcal{Q}_{\boldsymbol{\eta}}}{V\mathcal{Z}_0} \equiv \int \frac{\mathrm{d}\mathbf{r}}{V}\; p_{\boldsymbol{\eta}}^{\dagger}(\mathbf{r},0) \tag{84}$$

$$= \frac{R_\mathrm{e}^2}{6\pi^2}\left(\frac{1}{6\pi^2}\mathbb{\lambda}^{-1}\left\langle\boldsymbol{\eta}\boldsymbol{\eta}^{\mathrm{T}}\right\rangle_{\mathbb{\lambda}}\mathbb{\lambda}^{-1} - \mathbb{\lambda}^{-1}\right) \qquad \text{with} \qquad \langle\cdots\rangle_{\mathbb{\lambda}} \equiv \frac{\int \mathrm{d}\boldsymbol{\eta}\; W(\boldsymbol{\eta})\mathcal{Q}_{\boldsymbol{\eta}}\; \cdots}{\int \mathrm{d}\boldsymbol{\eta}\; W(\boldsymbol{\eta})\mathcal{Q}_{\boldsymbol{\eta}}} \tag{85}$$

This equation provides an implicit relation between the given, slow, collective variable $\mathbb{\chi}_1^2$ and the saddlepoint value of the auxiliary variable, $\mathbb{\lambda}[\omega_A,\omega_B,\mathbb{\chi}_1^2]$.

The assumption that $\mathbb{\lambda}$ does not vary in space also simplifies the saddlepoint condition, Equation 52, that relates the interaction fields, ω_A and ω_B, to the given density, $\phi_A(\mathbf{r})$:

$$\phi_A(\mathbf{r}) = \frac{\int \mathrm{d}\boldsymbol{\eta}\; W(\boldsymbol{\eta})\; \int_0^1 \mathrm{d}s\; \gamma_A(s)\; \left[\int \mathrm{d}\frac{\mathbf{r}_0}{R_\mathrm{e}^3}\; p_{\boldsymbol{\eta}}^{\mathbf{r}_0}(\mathbf{r},s)\right]\; p_{\boldsymbol{\eta}}^{\dagger}(\mathbf{r},s)}{\int \mathrm{d}\boldsymbol{\eta}\; W(\boldsymbol{\eta})\; \int \frac{\mathrm{d}\mathbf{r}_0}{V}\; p_{\boldsymbol{\eta}}^{\dagger}(\mathbf{r}_0,0)} \tag{86}$$

We therefore define the integrated single-chain propagator

$$\bar{p}_{\boldsymbol{\eta}}(\mathbf{r},s) \equiv \int \frac{\mathrm{d}\mathbf{r}_0}{R_\mathrm{e}^3}\; p_{\boldsymbol{\eta}}^{\mathbf{r}_0}(\mathbf{r},s) \tag{87}$$

which satisfies the modified diffusion equation, Equation 41, with the initial condition $\bar{p}_{\boldsymbol{\eta}}(\mathbf{r}, s) = 1$. In contrast to $p_{\boldsymbol{\eta}}^{\mathbf{r}_0}(\mathbf{r}, s)$, the integrated propagator, $\bar{p}_{\boldsymbol{\eta}}(\mathbf{r}, s)$, is a periodic function in space, like the interaction fields, ω_A and ω_B, as well as $p_{\boldsymbol{\eta}}^{\dagger}$. This periodicity allows us to confine the computation to a single unit cell of the periodic structure.

Using this definition of $\bar{p}_{\boldsymbol{\eta}}(\mathbf{r}, s)$, we obtain

$$\phi_A(\mathbf{r}) = \frac{\int \mathrm{d}\boldsymbol{\eta}\, W(\boldsymbol{\eta}) \int_0^1 \mathrm{d}s\, \gamma_A(s)\, \bar{p}_{\boldsymbol{\eta}}(\mathbf{r}, s) p_{\boldsymbol{\eta}}^{\dagger}(\mathbf{r}, s)}{\int \mathrm{d}\boldsymbol{\eta}\, W(\boldsymbol{\eta}) \int \frac{\mathrm{d}\mathbf{r}_0}{V}\, p_{\boldsymbol{\eta}}^{\dagger}(\mathbf{r}_0, 0)} = \left\langle \frac{V\mathcal{Z}_0}{\mathcal{Q}_{\boldsymbol{\eta}}} \int_0^1 \mathrm{d}s\, \gamma_A(s)\, \bar{p}_{\boldsymbol{\eta}}(\mathbf{r}, s) p_{\boldsymbol{\eta}}^{\dagger}(\mathbf{r}, s) \right\rangle_{\mathbb{\lambda}} \tag{88}$$

and the single-chain partition function, $\mathcal{Q}$, in Equation 48 takes the form

$$\mathcal{Q}_{\boldsymbol{\eta}} = e^{-\frac{\boldsymbol{\eta}^{\mathrm{T}}\boldsymbol{\eta}}{12\pi^2}} \int_{\hat{\mathbf{r}}(0)=\mathbf{r}_0} \mathcal{D}[\hat{\mathbf{r}}]\, e^{-\frac{3}{2R_{\mathrm{e}}^2}\int_0^1 \mathrm{d}s \left|\frac{\mathrm{d}\hat{\mathbf{r}}}{\mathrm{d}s}\right|^2} \times \exp\left(-\int_0^1 \mathrm{d}s \left[\omega(\hat{\mathbf{r}}(s), s) - \boldsymbol{\eta}^{\mathrm{T}} \frac{\hat{\mathbf{r}}(s)}{R_{\mathrm{e}}} \cos(\pi s)\right]\right) \tag{89}$$

$$\frac{\mathcal{Q}}{V\mathcal{Z}_0} = \int \mathrm{d}\boldsymbol{\eta}\, W(\boldsymbol{\eta}) \frac{\mathcal{Q}_{\boldsymbol{\eta}}}{V\mathcal{Z}_0} = \int \mathrm{d}\boldsymbol{\eta}\, W(\boldsymbol{\eta}) \int \frac{\mathrm{d}\mathbf{r}}{V}\, p_{\boldsymbol{\eta}}^{\dagger}(\mathbf{r}, 0) = \int \mathrm{d}\boldsymbol{\eta}\, W(\boldsymbol{\eta}) \int \frac{\mathrm{d}\mathbf{r}}{V}\, \bar{p}_{\boldsymbol{\eta}}(\mathbf{r}, 1) \tag{90}$$

Since $\mathbb{\lambda}$ does not depend on position, $\mathbf{r}$, and is symmetric, there is a coordinate system in which the matrix is diagonal, $\mathbb{\lambda} = \mathrm{diag}(\lambda_x, \lambda_y, \lambda_z)$. In this coordinate system, Equation 27 simplifies to

$$W(\boldsymbol{\eta}) = \prod_{\alpha=x,y,z} \frac{\exp\left(-\frac{1-\lambda_\alpha}{12\pi^2\lambda_\alpha}\eta_\alpha^2\right)}{\sqrt{12\pi^3\lambda_\alpha}} = \prod_{\alpha=x,y,z} \frac{1}{\sqrt{1-\lambda_\alpha}} \mathcal{N}\left(\eta_\alpha \middle| 0, \frac{6\pi^2\lambda_\alpha}{1-\lambda_\alpha}\right) \tag{91}$$

where $\mathcal{N}(\eta|\bar{\eta}, \sigma^2)$ is a Gaussian distribution of the variable η with average $\bar{\eta}$ and variance σ^2.

Often the given density, $\phi_A(\mathbf{r})$, is symmetric under spatial inversion, $\mathbf{r} \to -\mathbf{r}$ (after suitable choice of the coordinate origin). In this special case, also $\omega(\mathbf{r}, s) = \omega(-\mathbf{r}, s)$. The modified diffusion equations for $\bar{p}_{\boldsymbol{\eta}}(\mathbf{r}, s)$ and $p_{\boldsymbol{\eta}}^{\dagger}(\mathbf{r}, s)$ as well as the initial conditions remain invariant under the transformation, $\mathbf{r} \to -\mathbf{r}$ and $\boldsymbol{\eta} \to -\boldsymbol{\eta}$. Equation 89 asserts that $\mathcal{Q}_{\boldsymbol{\eta}}$ remains invariant under $\boldsymbol{\eta} \to -\boldsymbol{\eta}$, and also the weight $W(\boldsymbol{\eta})$ does not change under $\boldsymbol{\eta} \to -\boldsymbol{\eta}$. Therefore, we have to compute $\boldsymbol{\eta}$-dependent properties only for $\eta_x > 0$. In the case of chain compression, *i.e.*, $\lambda_\alpha < 0$ and $\eta_\alpha = i\bar{\eta}_\alpha$ being purely imaginary, space-inversion symmetry also guarantees that $\mathcal{Q}_{\boldsymbol{\eta}}$ is real-valued.

Random-Phase-Approximation (RPA)

The Random-Phase Approximation (RPA)[58] provides an approximate, analytical description of the lamellar phase by expanding around the spatially homogeneous system, see Spatially homogeneous system. For a given $\mathbb{\lambda}$, the sum over all single-chain conformations takes the form

$$\int \mathcal{D}[\hat{\mathbf{r}}]\mathcal{P}_{\mathbb{\lambda}}[\hat{\mathbf{r}}]\cdots \equiv \int \mathcal{D}[\hat{\mathbf{r}}]\mathcal{P}[\hat{\mathbf{r}}]\; e^{\frac{3\pi^2}{R_e^2}\hat{\mathbf{X}}_1^{\mathrm{T}}\mathbb{\lambda}\hat{\mathbf{X}}_1}\cdots = \int \mathrm{d}\hat{\mathbf{X}}_0\;\mathrm{d}\hat{\mathbf{X}}_1 e^{-\frac{3\pi^2}{R_e^2}\hat{\mathbf{X}}_1^{\mathrm{T}}[\mathbb{1}-\mathbb{\lambda}]\hat{\mathbf{X}}_1}\prod_{p=2}^{\infty}\mathrm{d}\hat{\mathbf{X}}_p\; e^{-\frac{3\pi^2}{R_e^2}p^2\hat{\mathbf{X}}_p^{\mathrm{T}}\hat{\mathbf{X}}_p}\cdots \tag{92}$$

and, in particular, we recover

$$\int \mathcal{D}[\hat{\mathbf{r}}]\mathcal{P}_{\mathbb{\lambda}}[\hat{\mathbf{r}}] = \frac{V\mathcal{Z}_0}{\sqrt{\det(\mathbb{1}-\mathbb{\lambda})}} \tag{93}$$

in agreement with Equation 70.

Defining the single-chain densities, $\hat{\rho}_A(\mathbf{r}) \equiv \int \mathrm{d}s\;\gamma_A(s)\delta\left[\mathbf{r}-\hat{\mathbf{r}}(s)\right]$ and similarly for $\hat{\rho}_B$, we expand Equation 13 with respect to the interaction fields, ω_A and ω_B, up to second order

$$\frac{\mathcal{Q}[\omega_A,\omega_B,\mathbb{\lambda}]\sqrt{\det(\mathbb{1}-\mathbb{\lambda})}}{V\mathcal{Z}_0} = \left\langle e^{-\int \mathrm{d}\mathbf{r}[\omega_A\hat{\rho}_A+\omega_B\hat{\rho}_B]}\right\rangle_{\mathbb{\lambda}} = \left\langle e^{-V\sum_{\mathbf{k}}\left[\omega_{-\mathbf{k},A}\hat{\rho}_{\mathbf{k},A}+\omega_{-\mathbf{k},B}\hat{\rho}_{\mathbf{k},B}\right]}\right\rangle_{\mathbb{\lambda}} \tag{94}$$

$$\approx e^{-\bar{\varepsilon}-\frac{1}{2}\sum_{\mathbf{k}\neq 0}\left[|\omega_{\mathbf{k},A}|^2 g^{\mathbb{\lambda}}_{\mathbf{k},AA}+2\omega_{-\mathbf{k},A}\omega_{\mathbf{k},B}g^{\mathbb{\lambda}}_{\mathbf{k},AB}+|\omega_{\mathbf{k},B}|^2 g^{\mathbb{\lambda}}_{\mathbf{k},BB}\right]} \tag{95}$$

and obtain the standard expression of the RPA with $\mathbb{\lambda}$-dependent, partial single-chain structure factors

$$g^{\mathbb{\lambda}}_{\mathbf{k},AA} = V^2\left\langle\hat{\rho}_{\mathbf{k},A}\hat{\rho}_{-\mathbf{k},A}\right\rangle_{\mathbb{\lambda}} = \left\langle\int \mathrm{d}s_1\gamma_A(s_1)\int \mathrm{d}s_2\;\gamma_A(s_2)\;e^{-i\mathbf{k}^{\mathrm{T}}[\hat{\mathbf{r}}(s_1)-\hat{\mathbf{r}}(s_2)]}\right\rangle_{\mathbb{\lambda}} \tag{96}$$

$$= \int \mathrm{d}s_1\gamma_A(s_1)\int \mathrm{d}s_2\gamma_A(s_2)\;e^{-\frac{\mathbf{k}^{\mathrm{T}}\mathbf{k}R_e^2}{6}|s_1-s_2|-\frac{R_e^2}{3\pi^2}\mathbf{k}^{\mathrm{T}}\left[\mathbb{\lambda}(\mathbb{1}-\mathbb{\lambda})^{-1}\right]\mathbf{k}\;[\cos(\pi s_1)-\cos(\pi s_2)]^2} \tag{97}$$

Similar expressions hold for the other partial single-chain structure factors.

The anisotropy of the distribution of single-chain conformations subjected to the tensorial orienting field, $\mathbb{\lambda}$, gives rise to an anisotropy of collective composition fluctuations. Within RPA, the inverse collective structure factor of composition fluctuations of a melt of diblock copolymers is

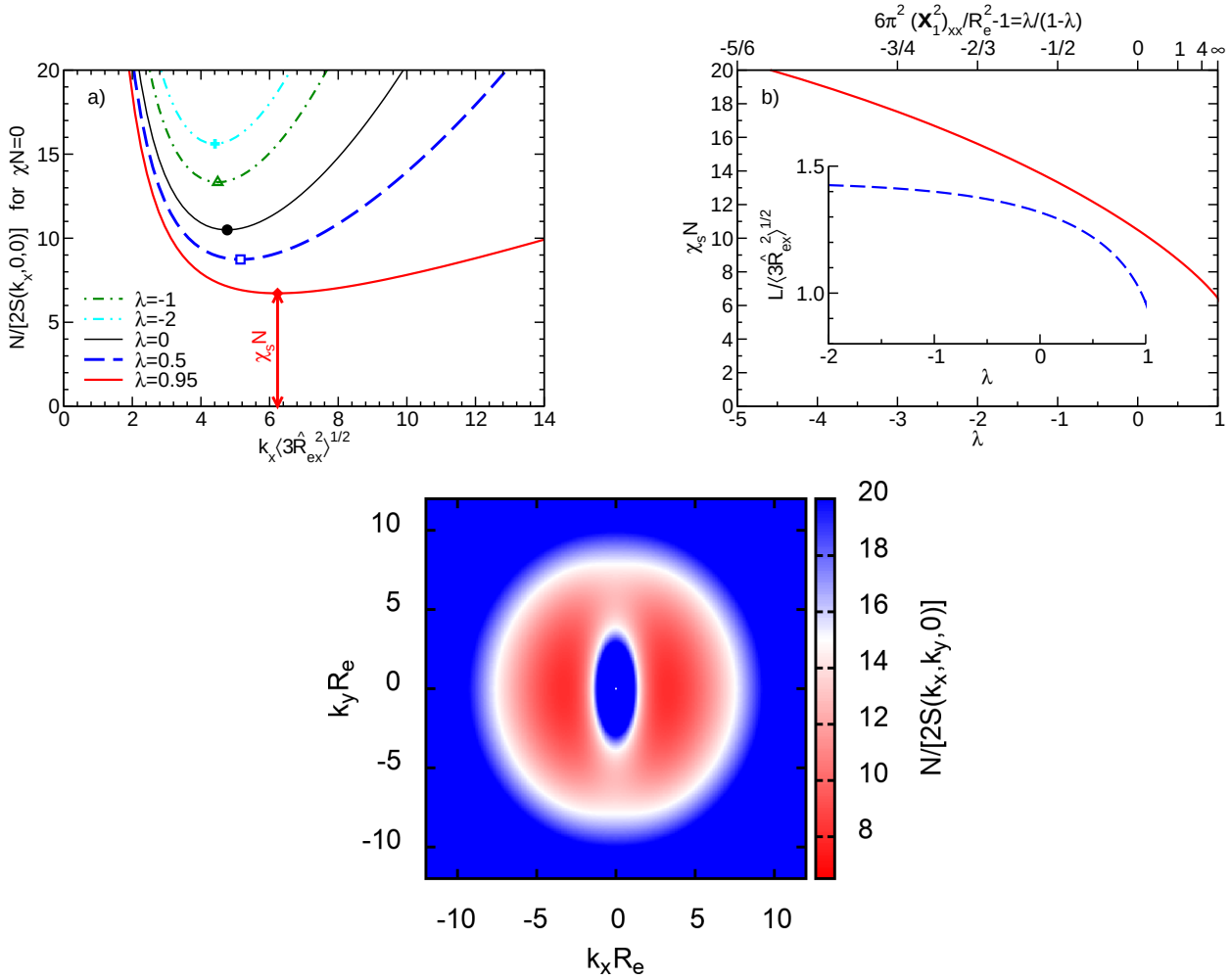

Figure 2: Collective scattering factor of a symmetric block copolymer for different $\lambda = \mathrm{diag}(\lambda, \lambda_y, \lambda_z)$ in the disordered phase.

a) Inverse collective structure factor, $N/[2S(k_x, 0, 0)]$, as a function of $k_x\sqrt{3\langle \hat{R}^2_{ex}\rangle}$ at $\chi N = 0$.

Note that for an isotropic Gaussian chain, $\sqrt{3\langle \hat{R}^2_{ex}\rangle} = R_e$. The minimum of the inverse collective structure factor yields the critical value of χN at the spinodal and the periodicity, L, of the emerging lamellar phase.

b) Critical incompatibility, $\chi_s N$, and lamellar period, L, measured in units of the stretched chain extension, $\sqrt{3\langle \hat{R}^2_{ex}\rangle}$, as a function of λ. The alternate abscissa shows the deviation of the variance of the first Rouse mode from its equilibrium value according to Equation 72.

c) Inverse scattering factor, $N/[2S(k_x, k_y, 0)]$, for $\lambda = \mathrm{diag}(0.675, -0.754116, \lambda_z)$ as a function of k_x and k_y.

given by[58]

$$\frac{N}{S(\mathbf{k})} = \frac{g^{\lambda}_{\mathbf{k},AA} + 2g^{\lambda}_{\mathbf{k},AB} + g^{\lambda}_{\mathbf{k},BB}}{g^{\lambda}_{\mathbf{k},AA}g^{\lambda}_{\mathbf{k},BB} - g^{\lambda\,2}_{\mathbf{k},AB}} - 2\chi N \tag{98}$$

Since $\mathbb{\lambda}$ is a symmetric 3×3 matrix, its eigenvalues are real and the eigendirections are orthogonal. Here we choose the coordinate system such that the eigendirections coincide with the Cartesian coordinates, x, y, and z. In Figure 2a we present the collective structure factor for wavevectors, $\mathbf{k} = k_x\mathbf{e}_x$, along an eigendirection, $\mathbf{e}_\lambda = \mathbf{e}_x$ of $\mathbb{\lambda}$ with eigenvalue λ. The spinodal instability of the homogeneous phase against spatial modulations of the composition along $\mathbf{e}_\lambda$ at incompatibility $\chi_s N$ is signaled by the zero of the inverse structure factor, *i.e.*,

$$\chi_s N(\mathbf{e}_\lambda) \equiv \frac{1}{2}\min_k \frac{g^{\mathbb{\lambda}}_{k\mathbf{e}_\lambda,AA} + 2g^{\mathbb{\lambda}}_{k\mathbf{e}_\lambda,AB} + g^{\mathbb{\lambda}}_{k\mathbf{e}_\lambda,BB}}{g^{\mathbb{\lambda}}_{k\mathbf{e}_\lambda,AA}g^{\mathbb{\lambda}}_{k\mathbf{e}_\lambda,BB} - g^{\mathbb{\lambda}\,2}_{k\mathbf{e}_\lambda,AB}} \tag{99}$$

The order-disorder transition (ODT) occurs at $\chi_{\mathrm{ODT}}N = \min_{\mathbf{e}_\lambda}\chi_s N(\mathbf{e}_\lambda)$, and the eigendirection, $\mathbf{e}^*_\lambda$, for which the minimum is attained, is the thermodynamically preferred direction of lamella normals. Figure 2a illustrates that this instability shifts to smaller values of incompatibility, χN, as we increase the strength of the orienting field, λ. The characteristic wavevector of the emerging lamellar phase, in turn, slightly increases when measure in units of the inverse chain extension, $\sqrt{\langle\hat{R}^2_{ex}\rangle}$, *cf.* Equation 80, in the disordered phase with constrained variance of the first Rouse mode. The location of the ODT and the ratio of the emerging lamellar spacing in units of the nonequilibrium chain extension in the disordered phase is presented in Figure 2b. Upon increasing $(\mathbb{X}^2_1)_{xx}$, we observe that the critical incompatibility decreases to about $\chi_{\mathrm{ODT}}N \approx 6.5$. This values agrees with the result of a partial-enumeration calculation[59] for $\lambda = 1 - \frac{1}{6\pi^2} \approx 0.983$. The length scale of the emerging lamellar phase at the ODT approaches $L^* \approx 0.97\sqrt{3\langle\hat{R}^2_{ex}\rangle}$ in the limit of strong stretching, $\lambda \to 1$, *i.e.*, the lamellar spacing increases with λ but less so than the corresponding component of the root mean-squared end-to-end vector.

Figure 2c presents the inverse, collective scattering factor $N/[2S(\mathbf{k})]$ in the disordered phase, $\chi N = 0$, for an anisotropic orienting field, $\mathbb{\lambda}$. The chosen orienting field corresponds to a system that, starting from an equilibrated melt of symmetric Gaussian copolymers, has been affinely stretched along the x-direction by a factor $\epsilon = 1/\sqrt{1-\lambda}$ with $\lambda = \lambda_x = 0.675$ and compressed in the y-direction by a factor $1/\sqrt{\epsilon}$ corresponding to $\lambda_y = 1 - 1/\sqrt{1-\lambda} = -0.754116$. As expected,

fluctuations along the stretching direction are enhanced and the maximum of the scattering occurs at a smaller wavevector along the stretching direction, x, than along the orthogonal one.

One-dimensional density variation

In the following, we consider a lamellar phase formed by symmetric diblock copolymers or multiblock copolymers. In this case, the density $\phi_A(\mathbf{r})$ varies only in a single spatial direction, x. The same holds true for $\bar{p}_{\boldsymbol{\eta}}$, $p^\dagger_{\boldsymbol{\eta}}$, and the saddlepoint fields, ω_A and ω_B.[4] Equation 41 also implies that $\bar{p}_{\boldsymbol{\eta}}$ and $p^\dagger_{\boldsymbol{\eta}}$ only depend on the x component, η_x, of $\boldsymbol{\eta}$.

Given $\omega_A(x)$, $\omega_B(x)$, and $\mathbb{\lambda}$, we obtain the single-chain partition function, Equation 48,

$$\frac{\mathcal{Q}}{V\mathcal{Z}_0} = \int \mathrm{d}\eta_x W_x(\eta_x)\mathcal{Q}_{\eta_x} = \int \mathrm{d}\eta_x W_x(\eta_x) \int \frac{\mathrm{d}x}{L_x}\, p^\dagger_{\eta_x}(x,0) = \int \mathrm{d}\eta_x W_x(\eta_x) \int \frac{\mathrm{d}x}{L_x}\, \bar{p}_{\eta_x}(x,1) \quad (100)$$

and the normalized density of A segments

$$\phi_A(x) = \frac{\int \mathrm{d}\eta_x\; W_x(\eta_x)\; \int_0^1 \mathrm{d}s\; \gamma_A(s)\bar{p}_{\eta_x}(x,s)p^\dagger_{\eta_x}(x,s)}{\int \mathrm{d}\eta_x\; W_x(\eta_x)\; \int \frac{\mathrm{d}x_0}{L_x}\; p^\dagger_{\eta_x}(x_0,0)} \quad (101)$$

where L_x is the system size in the x direction and

$$W_x(\eta_x) = \int \mathrm{d}\boldsymbol{\eta}_\perp\; W(\boldsymbol{\eta}) = \frac{\int \mathrm{d}\boldsymbol{\eta}_\perp\; \exp\left(-\frac{\boldsymbol{\eta}^{\mathrm{T}}\left[\mathbb{\lambda}^{-1}-\mathbb{1}\right]\boldsymbol{\eta}}{12\pi^2}\right)}{\sqrt{\det(12\pi^3\mathbb{\lambda})}} \quad (102)$$

Simultaneously inverting Equation 101, a similar equation for the the density of B segments, $1-\phi_A$, and Equation 85, we obtain the saddlepoint values, ω_A, ω_B, and $\mathbb{\lambda}$ of the auxiliary fields, Ω_A, Ω_B, and $\mathbb{\Lambda}$. The insertion of the so-determined saddlepoint values in Equation 19 yields the free energy, $\mathcal{F}[\phi_A, \mathbb{X}_1^2]$, as a functional of the two slow variables, density and variance of the first Rouse modes.

In the following, we additionally assume that the density relaxes to its equilibrium for the given

[4] In a one-dimensional system, the propagator $p^{\mathbf{r}_0}_{\boldsymbol{\eta}}$ is given by $p^{\mathbf{r}_0}_{\boldsymbol{\eta}}(\mathbf{r},s) = p^{x_0}_{\eta_x}(x,s) \times \left(\frac{3}{2\pi s}\right) \exp\left(-\frac{3}{2s}\left[\frac{\mathbf{r}_\perp - \mathbf{r}_{0\perp}}{R_\mathrm{e}} - \frac{\boldsymbol{\eta}_\perp}{3\pi^2}\left\{\cos(\pi s)-1\right\}\right]^2\right)$.

variance of the first Rouse modes, $\mathbb{X}_1^2$. Using the corresponding saddlepoint equation, Equation 21, we rewrite the free energy in the simple form

$$\frac{\mathcal{G}[\mathbb{\lambda}]}{k_{\mathrm{B}}T\sqrt{\bar{\mathcal{N}}}V/R_{\mathrm{e}}^3} = \ln\frac{n}{eV\mathcal{Z}_0} - \ln\frac{\mathcal{Q}}{V\mathcal{Z}_0} - \chi N\int\frac{\mathrm{d}\mathbf{r}}{V}\,\phi_A(1-\phi_A) \tag{103}$$

$$\frac{\mathcal{F}[\mathbb{X}_1^2]}{k_{\mathrm{B}}T\sqrt{\bar{\mathcal{N}}}V/R_{\mathrm{e}}^3} = \frac{\mathcal{G}[\mathbb{\lambda}]}{k_{\mathrm{B}}T\sqrt{\bar{\mathcal{N}}}V/R_{\mathrm{e}}^3} + \frac{3\pi^2}{R_{\mathrm{e}}^2}\mathbb{\lambda}:\mathbb{X}_1^2 \tag{104}$$

depending on whether $\mathbb{\lambda}$ or $\mathbb{X}_1^2$ is used as the independent thermodynamic variable. In the latter case, the value of the tensorial, orienting field, $\mathbb{\lambda}$, is implicitly given by Equation 85.

In the following, we consider the important special case where the x-direction, *i.e.*, the lamella normal, coincides with one eigenvector of the matrix $\mathbb{\lambda}$. We denote by $\lambda = \lambda_x$ the corresponding eigenvalue of $\mathbb{\lambda}$. Working in the eigenbasis, where the other eigendirections are y and z, the variance of the first Rouse modes is then given by

$$\mathbb{X}_1^2 = \frac{R_{\mathrm{e}}^2}{6\pi^2}\frac{\int\mathrm{d}\eta_x\, e^{-\frac{1-\lambda}{12\pi^2\lambda}\eta_x^2}\mathcal{Q}_{\eta_x}\int\mathrm{d}\eta_y\mathrm{d}\eta_z\, e^{-\frac{1-\lambda_y}{12\pi^2\lambda_y}\eta_y^2}e^{-\frac{1-\lambda_z}{12\pi^2\lambda_z}\eta_z^2}\left(\frac{1}{6\pi^2}\mathbb{\lambda}^{-1}\boldsymbol{\eta}\boldsymbol{\eta}^{\mathrm{T}}\mathbb{\lambda}^{-1}-\mathbb{\lambda}^{-1}\right)}{\int\mathrm{d}\eta_x\, e^{-\frac{1-\lambda}{12\pi^2\lambda}\eta_x^2}\mathcal{Q}_{\eta_x}\int\mathrm{d}\eta_y\mathrm{d}\eta_z\, e^{-\frac{1-\lambda_y}{12\pi^2\lambda_y}\eta_y^2}e^{-\frac{1-\lambda_z}{12\pi^2\lambda_z}\eta_z^2}} \tag{105}$$

$$= \mathrm{diag}\left(\left(\mathbb{X}_1^2\right)_{xx}, \frac{R_{\mathrm{e}}^2}{6\pi^2(1-\lambda_y)}, \frac{R_{\mathrm{e}}^2}{6\pi^2(1-\lambda_z)}\right) \tag{106}$$

with the nontrivial component being

$$\left(\mathbb{X}_1^2\right)_{xx} = \frac{R_{\mathrm{e}}^2}{6\pi^2}\frac{\int\mathrm{d}\eta_x\, e^{-\frac{1-\lambda}{12\pi^2\lambda}\eta_x^2}\mathcal{Q}_{\eta_x}\left(\frac{\eta_x^2}{6\pi^2\lambda^2}-\frac{1}{\lambda}\right)}{\int\mathrm{d}\eta_x\, e^{-\frac{1-\lambda}{12\pi^2\lambda}\eta_x^2}\mathcal{Q}_{\eta_x}} \tag{107}$$

Moreover, we obtain a simple expression for $W_x(\eta_x)$ from Equation 102

$$W_x(\eta_x) = \frac{\exp\left(-\frac{1-\lambda}{12\pi^2\lambda}\eta_x^2\right)}{\sqrt{12\pi^3\lambda(1-\lambda_y)(1-\lambda_z)}} \tag{108}$$

In Figure 3a we present numerical data for $\mathcal{Q}_{\eta_x} \equiv \int\frac{\mathrm{d}x}{L_x}\,\bar{p}_{\eta_x}(x,1)$ in the lamellar phase of a symmetric diblock at $\chi N = 20$, $\lambda = 0.675$, and its optimal lamellar spacing, $L = 2.399R_{\mathrm{e}}$. Figure 3a shows $\mathcal{Q}_{\eta_x}$ as a function of η_x. For the inversion-symmetric lamellar phase, $\mathcal{Q}_{\eta_x} = \mathcal{Q}_{-\eta_x}$, and only

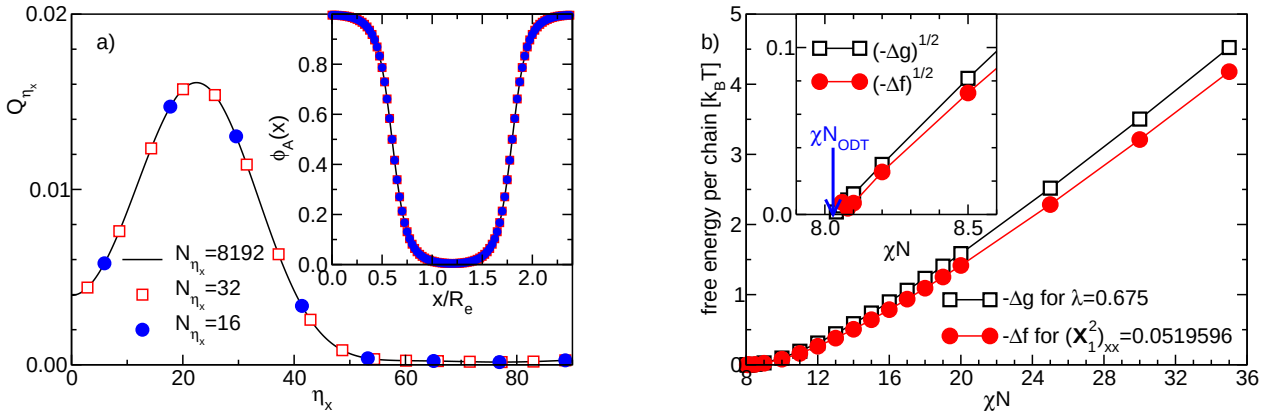

Figure 3: a) Single-chain partition function, $\mathcal{Q}_{\eta_x} = \mathcal{Q}_{-\eta_x}$, from Equation 100, as a function of η_x. Sample points used to evaluate integrals over the auxiliary variable, η_x, for $N_{\eta_x} = 16$ and 32 are marked; $N_{\eta_x} = 8192$ gives an effectively continuous line. Parameter values: $\lambda = 0.675$, $\chi N = 20$ and $L = 2.399 R_e$. Inset: Equilibrated $\phi_A(x)$, for the three different N_{η_x}, showing that even $N_{\eta_x} = 32$ is large enough here to obtain effectively converged results, characteristic for $N_{\eta_x} \to \infty$. b) Free energy differences per chain – Δg for a given $\lambda = 0.675$ or Δf for a given $(\mathbb{X}_1^2)_{xx} = 0.0519596 R_e^2$ – of a symmetric diblock copolymer as a function of incompatibility, χN, with respect to the disordered phase. The inset presents the square root of the free-energy differences. The arrow marks the ODT as predicted by RPA.

nonnegative values of η_x are presented. [5]

The integral over η_x is discretized into a finite number of sampling points, N_{η_x}, as also illustrated in Figure 3a. The actual dependence on N_{η_x} appears to be rather weak, however, so that quite moderate values of N_{η_x} are sufficient (*cf.*, inset of Figure 3a).

In the general case, the computationally heavy part of the calculation is the solution of the modified diffusion equation, Equation 41, for the different sampling points of $\boldsymbol{\eta}$ and $\mathbf{r}_0$. These calculations can be performed independently and are well suited for parallel computers. Only the partial results for the single-chain partition function, Equation 48, and the densities, Equation 52, at fixed sampling points of $\boldsymbol{\eta}$ and $\mathbf{r}_0$ have to be combined in each iteration that adjusts the fields, ω_A, ω_B, and $\mathbb{\lambda}$, towards the saddlepoint, Equation 15–17. Thus, in the case where the densities vary in three dimensions but the molecular conformations are uniformly deformed in two dimensions x

[5] In calculations of the density one can explicitly enforce $\phi_A(x) = \phi_A(-x)$ and restrict the integral in Equation 101 to only $\eta_x \geq 0$.

and y (*e.g.*, planar elongation or shear flow), the calculation is a factor of $N_{\eta_x}N_{\eta_y} \sim \mathcal{O}(10^2)$ slower than an equilibrium SCFT calculation but the calculations can be straightforwardly distributed over $N_{\eta_x}N_{\eta_y}$ processors. If, however, the molecular conformations, $\mathbb{X}_1^2(\mathbf{r})$, vary in space also the integral over $\mathbf{r}_0$ needs to be discretized, adding significantly to the computational cost.

In Figure 3b we plot the difference between the free energy, $\mathcal{G}$, per chain in units of $k_\mathrm{B}T$ and the corresponding quantity of the disordered phase, for $\lambda = 0.675$ as a function of the incompatibility, χN. The free-energy difference vanishes quadratically at the ODT, as expected for a second-order phase transition of the symmetric copolymer melt within a mean-field approximation. The graph also depicts the free-energy difference $\Delta f = \frac{\mathcal{F}-\mathcal{F}_\mathrm{hom}}{k_\mathrm{B}T\sqrt{\mathcal{N}}V/R_\mathrm{e}^3}$ at fixed $(\mathbb{X}_1^2)_{xx} = \frac{R_\mathrm{e}^2}{6\pi^2(1-\lambda)} \approx 0.0519596R_\mathrm{e}^2$ as a function of incompatibility, exhibiting a similar quadratic dependency. Since the value of the variance of the first Rouse mode, $(\mathbb{X}_1^2)_{xx}$ is related to $\lambda = 0.675$ via the constitutive relation, Equation 72, of the disordered phase, the ODTs of the two systems coincide.

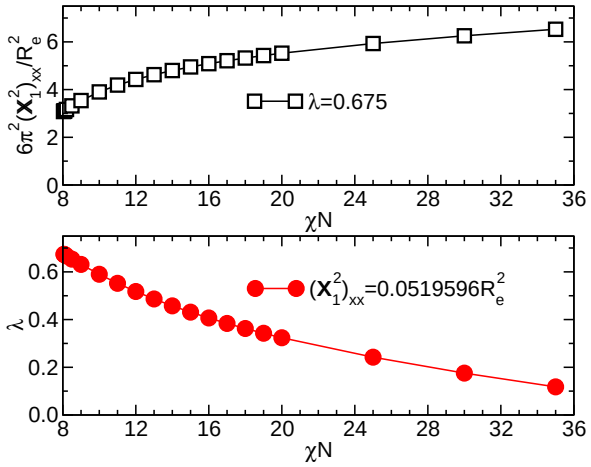

Figure 4: top: Variance, $(\mathbb{X}_1^2)_{xx}$, of the first Rouse mode as a function of χ at fixed $\lambda = 0.675$. bottom: Saddlepoint value, λ, as a function of χN at fixed $(\mathbb{X}_1^2)_{xx}$.

The constitutive relation between λ and $(\mathbb{X}_1^2)_{xx}$ for the homogeneous phase is given by the simple analytic expression, Equation 72. The lamellar ordering will modify this relation. In the top panel of Figure 4, we plot the variance of the first Rouse mode, $(\mathbb{X}_1^2)_{xx}$, in the lamellar phase as a function of the incompatibility, χN, at a fixed value of $\lambda = 0.675$ and the optimal, χN-dependent value of L. As we increase χN, the stretching of the molecular conformations along the lamella normal increases and so does the variance of the first Rouse mode, $(\mathbb{X}_1^2)_{xx}$. In the bottom panel

of Figure 4, we plot λ as a function of the incompatibility, χN, in the lamellar phase for a given $(\mathbb{X}_1^2)_{xx} = 0.0519596 R_e^2$. Since the block copolymers stretch for larger χN, a smaller value of λ is required to achieve the given value of $(\mathbb{X}_1^2)_{xx} > \frac{R_e^2}{6\pi^2}$.

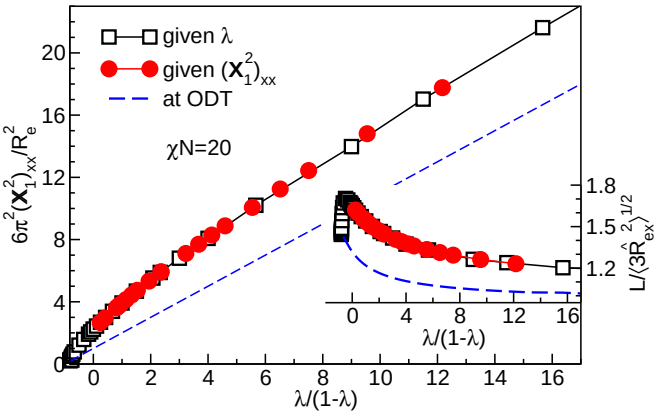

Figure 5: $(\mathbb{X}_1^2)_{xx}$ as a function of λ at fixed $\chi N = 20$. The dashed line is the prediction for disordered phase, Equation 72. Inset: Lamellar spacing, L, as a function of λ at fixed $\chi N = 20$. The dashed line depicts the lamellar spacing at the ODT predicted by RPA.

In Figure 5 we compare the constitutive relation that relates $(\mathbb{X}_1^2)_{xx}$ and λ, between the lamellar phase at $\chi N = 20$ and the disordered phase. The figure depicts two data sets. First, we fix λ, calculate the properties of the lamellar phase by minimizing $\mathcal{G}$ with respect to the lamellar period, and then calculate $(\mathbb{X}_1^2)_{xx}$ according to Equation 107. Second, we fix $(\mathbb{X}_1^2)_{xx}$ by adjusting λ and then calculate the properties of the lamellar phase by minimizing $\mathcal{F}$ with respect to the lamellar period. Gratifyingly, both procedures agree and the corresponding values for the optimal lamellar spacing, L, are shown in the inset of Figure 5. The ratio $L/\sqrt{3\langle R_{e,x}^2\rangle}$ is nonmonotonic in the vicinity of the ODT, *i.e.*, $\lambda \approx -4.5853$ at $\chi N = 20$; in units of R_e, however, the lamellar spacing increases. The value $L \approx 7.71 R_e$ for $\lambda = 0.983$ is compatible with the result $L \approx 7.6 R_e$ obtained by the previous partial enumeration calculation[59] using 99 840 000 chains of 64 beads, each. The latter calculation, however, required orders of magnitude more computational resources. The constitutive relation in the lamellar phase and the disordered phase are qualitatively similar. At a fixed λ, the variance of the first Rouse mode is always larger in the lamellar phase than in the disordered one, because of the chain stretching along the normals of the internal AB interfaces. For $\lambda \to 1$, $(\mathbb{X}_1^2)_{xx}$ diverges in both phases.

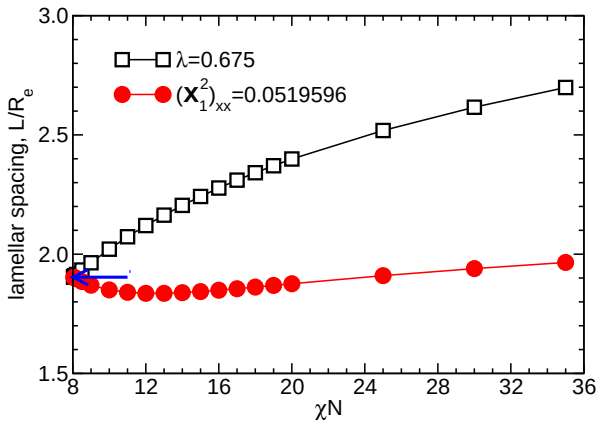

Figure 6: Lamellar spacing, L, as a function of χN at fixed $\lambda = 0.675$ (open squares) or $(\mathbb{X}_1^2)_{xx} = 0.0519596 R_e^2$ (filled circles), *cf.*, Figure 4. Since the fixed values of λ and $(\mathbb{X}_1^2)_{xx}$ are related by the constitutive equation of the disordered phase, the ODTs of both systems coincide. The arrow marks the lamellar spacing at the ODT, predicted by the RPA .

Figure 6 presents the lamellar spacing, L, as function of incompatibility, χN. At a given $\lambda = 0.675$ we minimize $\mathcal{G}$ to obtain the lamellar spacing, L, and find that L increases with incompatibility. Fixing λ, we basically alter the underlying distribution of chain conformations, *i.e.*, we use a nongaussian, stretched copolymer architecture in the absence of nonbonded interactions. In the lamellar phase, the behavior is qualitatively similar to that of an unconstrained copolymer, where the lamellar spacing is dictated by a balance of the free energy of the internal AB interfaces and the entropy loss due to molecular stretching at large χN. Thus, the lamellar spacing, L, monotonously increases with incompatibility, and it is always larger than for a Gaussian chain, $\lambda = 0$.

The χN-dependence of the lamellar spacing at fixed variance, $(\mathbb{X}_1^2)_{xx}$, of the first Rouse mode is qualitatively different. In the strong segregation limit, $\chi N \gg \chi_{\mathrm{ODT}} N$, the interfacial tension, γ_{AB} between A and B domains is not expected to be significantly affected by the constraint on $(\mathbb{X}_1^2)_{xx}$ and increases with χN, similar to that of a Gaussian diblock copolymer because γ_{AB} is determined by the small-scale statistics of short loops of A blocks in the B domain and *vice versa*. Fixing $(\mathbb{X}_1^2)_{xx}$, however, we effectively prevent the large-scale chain conformations from responding to an increase of incompatibility, *i.e.*, the constraint of the variance of the first Rouse mode does not allow the chains to stretch and thereby increase L. Thus, L increases only very weakly with χN at large incompatibility.

In the vicinity of the ODT, the system with fixed $(\mathbb{X}_1^2)_{xx}$ behaves similar to an unconstrained system of copolymers that are characterized by an underlying nongaussian, λ-dependent copolymer architecture in the absence of nonbonded interactions. The size of these corresponding unconstrained copolymers, however, shrinks with χN because λ decreases with χN, as shown in Figure 4. The lamellar spacing upon increase of χN is determined by an increase of L in units of the λ-dependent end-to-end distance of the corresponding unconstrained copolymers and a decrease of this unit because of the dependence of λ on χN. The interplay between these two counteracting effects largely cancel to keep $(\mathbb{X}_1^2)_{xx}$ independent of χN, resulting in a minor, nonmonotonic variation of the lamellar spacing in the vicinity of the ODT.

Lamellar phase of symmetric multiblock copolymers – Relation between fraction of bridges and the variance of the first Rouse mode

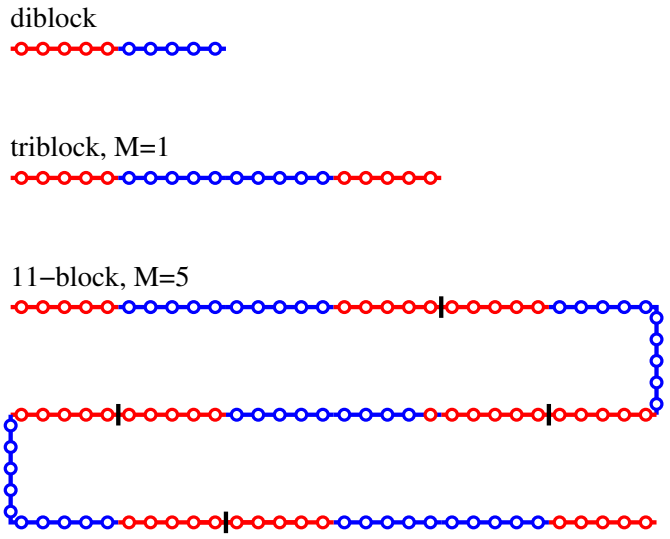

Figure 7: Illustration of diblock copolymer, triblock copolymer ($M = 1$) and 11-block copolymer ($M = 5$) with $N_{\mathrm{db}} = 10$.

In the following we consider a melt of symmetric multiblock copolymer with architecture $(ABBA)_M$, as illustrated in Figure 7. Each multiblock copolymer is comprised of $2N_{\mathrm{db}}M$ segments. The equilibrium phase behavior is analogous to that of symmetric diblock copolymers of length N_{db}. In the limit $M \to \infty$, the melt will form a lamellar phase for $\chi N_{\mathrm{db}} > 7.55$[40] with a lamellar period that is proportional to the spatial extent of a block, $L \sim b\sqrt{N_{\mathrm{db}}} = R_{\mathrm{e}}/\sqrt{2M}$. Again, we

study a one-dimensional variation of the density, $\phi_A(x)$.

The conformation of a multiblock copolymer in a lamellar phase can be conceived as a sequence of loops and bridges. A loop consists of a block whose two end segments are located on the same internal AB interface. A bridge, in turn, straddles a domain and the end segments of the block are located on neighboring interfaces. Since converting loops into bridges or *vice versa* requires a block to move across the domain of the opposite species, it involves a large free-energy barrier, $\Delta F \sim k_{\rm B}T\chi N_{\rm db}$, for the *single-chain dynamics*. Thus, the relaxation of loops and bridges in a segregated lamellar phase is extremely slow. Simulations indicate that the bridge fraction, $\nu_{\rm B}$, is determined in the course of microphase separation and often remains below its equilibrium value predicted by SCFT.[44] This nonequilibrium behavior is expected because the formation of the microphase-separated morphology occurs on the Rouse relaxation time of a block, whereas the relaxation of the overall chain conformation (and thereby the equilibration of loops and bridges) is dictated by the Rouse time of the entire multiblock, which is a factor M^2 longer. Thus, strongly segregated multiblock copolymers are likely not to reach equilibrium, being characterized instead by a nonequilibrium value of $\nu_{\rm B}$. The latter is then a slow, collective variable that characterizes the nonequilibrium chain conformations. In the following, we explore the correlation between the bridge fraction, $\nu_{\rm B}$, and the variance, $\langle \hat{X}_{1x}\hat{X}_{1x}\rangle$, of the first Rouse mode.

A multiblock is comprised of $2M\nu_{\rm B}$ bridges on average. We associate with each bridge a spin variable, $\sigma_i = \pm 1$, depending on the sign of the distance, $\hat{x}(s+\delta s)-\hat{x}(s) \approx \pm L/2$ with $\delta s = N_{\rm db}/N$. The alternating structure of lamellar domains in space and the alternating sequence of A and B blocks along the chain contour gives rise to a correlation between the direction of neighboring bridges, *i.e.*, the spin variable of neighboring bridges will have the same sign, if they are separated by an even number of loops. Conversely, $\sigma_{i+1}\sigma_i = -1$ if the two bridges are separated by an odd number of loops. In the limit of many blocks, $M \to \infty$, this gives rise to an Ising-like, exponential correlation[44]

$$\langle \sigma_i \sigma_j \rangle \overset{M\to\infty}{=} \left(\frac{\nu_{\rm B}}{2-\nu_{\rm B}} \right)^{|i-j|} \tag{109}$$

Conceiving the conformation of multiblock copolymers as a persistent one-dimensional random

walk, we derive an approximate relation between the variance of the first Rouse mode, $\langle \hat{X}_{1x}\hat{X}_{1x}\rangle$, and the fraction of bridges, ν_{B} in the limit $M \gg 1$. Ignoring fluctuations of the position of a bridge along the chain contour, we associate the i^{th} bridge with contour position $s_i = \frac{i}{2\nu_{\mathrm{B}}M}$. If we let $\hat{x}(0)$ denote the starting position of the multiblock, then the spatial position, $\hat{x}_i \approx \hat{x}(s_i)$ of the i^{th} bridge is given by $\hat{x}(s_i) \approx \hat{x}_i \approx \hat{x}(0) + \frac{L}{2}\sum_{n<i}\sigma_n$. Using Equation 109, we compute the correlation of bridge positions

$$\langle [\hat{x}(s_i) - \hat{x}(0)][\hat{x}(s_j) - \hat{x}(0)]\rangle = \frac{L^2}{4}\sum_{n<i}\sum_{m<j}\langle \sigma_n\sigma_m\rangle \approx \frac{L^2}{4}\min(i,j)\sum_{\delta=-\infty}^{\infty}\left(\frac{\nu_{\mathrm{B}}}{2-\nu_{\mathrm{B}}}\right)^{|\delta|} \tag{110}$$

$$= \frac{\nu_{\mathrm{B}}ML^2}{2(1-\nu_{\mathrm{B}})}\min(s_i,s_j) \tag{111}$$

In particular, we obtain for the mean, squared end-to-end distance $\langle \hat{R}^2_{\mathrm{e}x}\rangle \approx \frac{\nu_{\mathrm{B}}ML^2}{2(1-\nu_{\mathrm{B}})}$.[44] The spatial correlation of the bridge positions also allows us to compute the variance of the first Rouse mode

$$\left\langle \hat{X}_{1x}\hat{X}_{1x}\right\rangle \approx \int \mathrm{d}s_1 \int \mathrm{d}s_2 \, \frac{\nu_{\mathrm{B}}ML^2}{2(1-\nu_{\mathrm{B}})}\min(s_1,s_2)\,\cos(\pi s_1)\cos(\pi s_2) \tag{112}$$

$$= \frac{\nu_{\mathrm{B}}ML^2}{2(1-\nu_{\mathrm{B}})}\,2\int_0^1 \mathrm{d}s_1\,\cos(\pi s_1)\int_0^{s_1}\mathrm{d}s_2\; s_2\cos(\pi s_2) = \frac{\nu_{\mathrm{B}}ML^2}{4\pi^2(1-\nu_{\mathrm{B}})} \tag{113}$$

i.e., by specifying the variance of the first Rouse modes, $\mathbb{X}_1^2$, we can control the fraction of bridges and drive ν_{B} away from its equilibrium value. Using Equation 81 to identify $\langle \hat{X}_{1x}\hat{X}_{1x}\rangle$ and $(\mathbb{X}_1^2)_{xx}$, we obtain

$$\nu_{\mathrm{B}} \approx \frac{(\mathbb{X}_1^2)_{xx}}{(\mathbb{X}_1^2)_{xx} + \frac{ML^2}{4\pi^2}} \tag{114}$$

Within this approximation, the variance of the first Rouse mode and the mean, squared end-to-end distance of the multiblock copolymer in the lamellar phase have the same dependence on the fraction of bridges, *i.e.*, $\langle \hat{R}^2_{\mathrm{e}x}\rangle \approx 2\pi^2\left\langle \hat{X}_{1x}\hat{X}_{1x}\right\rangle$. This relation indicates that $\langle \hat{R}^2_{\mathrm{e}x}\rangle$ at constrained $\left\langle \hat{X}_{1x}\hat{X}_{1x}\right\rangle = (\mathbb{X}_1^2)_{xx}$ is slightly larger than in a spatially homogeneous system, $\langle \hat{R}^2_{\mathrm{e}x}\rangle = 16\left\langle \hat{X}_{1x}\hat{X}_{1x}\right\rangle + \left(\frac{1}{3} - \frac{16}{6\pi^2}\right)R_{\mathrm{e}}^2$, according to Equation 80. The increase of the prefactor arises from correlations along the persistent random walk; in the limit a rod-like polymer the prefactor rises to

$$\langle \hat{R}_{ex}^2 \rangle / \langle \hat{X}_{1x} \hat{X}_{1x} \rangle = \pi^4/4 \approx 24.35.$$

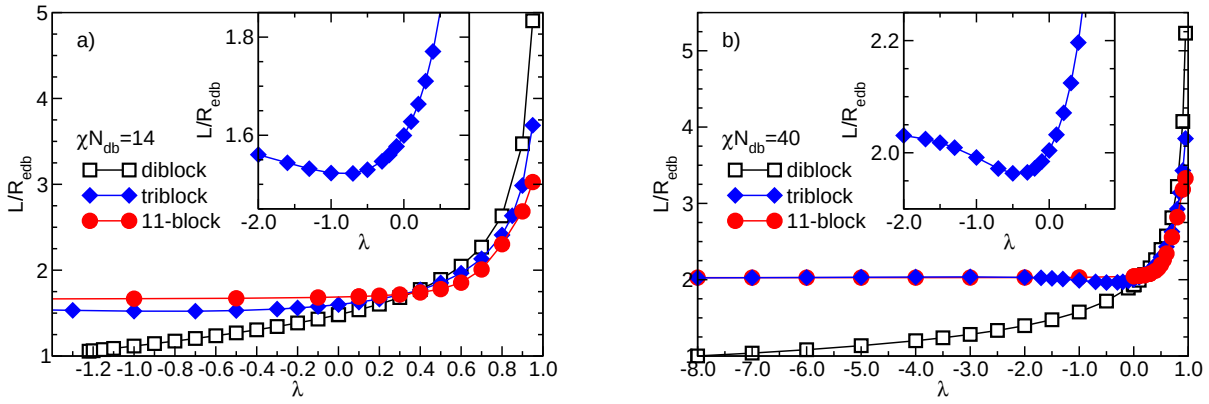

Figure 8: Comparison of the lamellar spacing, L, for a symmetric 11-block copolymer ($M = 5$) at $\chi N_{11-\mathrm{block}} = 140$ and 400, a symmetric triblock ($M = 1$) at $\chi N_{3-\mathrm{block}} = 28$ and 80, and a symmetric diblock at $\chi N_{\mathrm{db}} = 14$ and 40. L is always measured in units of the size,R_{edb}, of the corresponding diblock copolymer *i.e.*, R_{e} for the diblock copolymer and $R_{e,M-\mathrm{block}}/\sqrt{2M}$ for the multiblock copolymers. Inset: Nonmonotonic dependence of optimal lamellar spacing on the strength of the orienting field, λ, for the triblock system.

In Figure 8 we compare the lamellar spacing of symmetric diblock copolymers, symmetric triblocks, $M = 1$, and symmetric 11-block copolymers, $M = 5$, for $\chi N_{\mathrm{db}} = 14$ and 40, of the diblock copolymer and a factor $\frac{\chi N_{11-\mathrm{block}}}{\chi N_{\mathrm{db}}} = 2M$ larger for the multiblocks. For the diblock with $\chi N_{\mathrm{db}} = 14$, the lamellar phase transitions to the disordered phase around $\lambda = -1.275$.

For the diblock and the 11-block copolymers, the lamellar spacing, L, increases with λ. The response to stretching, $\lambda > 0$, or compression, $\lambda < 0$, however, is much less pronounced for the 11-block than it is for the diblock copolymer. Qualitatively, increasing λ stretches the overall chain conformations but larger length scales are affected more strongly than shorter ones. In a diblock copolymer, increasing λ directly affects the spatial extent of a block and thereby the lamellar spacing, L. In a multiblock copolymer, however, λ, chiefly affects the statistics of loops and bridges, *i.e.*, the arrangement of blocks in space rather than the spatial extent of an individual block. [6]

[6]The situation for $\lambda > 0$ is reminiscent of the Pincus blob picture[60] of a stretched linear chain with a constrained end-to-end distance $R_c > R_{\mathrm{e}}$. Inside a blob of size ξ, the chain statistics remains Gaussian and isotropic, whereas the blobs are arranged linearly in space. Upon increasing the spatial extent R_c, the blob size, $\xi = R_{\mathrm{e}}^2/R_c$, which characterizes the fluctuation perpendicular to the constrained end-to-end vector, decreases, and only once it reaches $\xi \sim L$ is the lamellar spacing affected significantly.

The inset of Figure 8 reveals a slightly nonmonotonic dependence of the lamellar spacing, L, on λ for compressed triblock copolymers, *i.e.*, the lamellar spacing decreases as the compression of the triblock copolymers is reduced. We attribute this behavior to the observation that compressed chains form more loops and fewer bridges than stretched chains and that bridges, which straddle lamellar domains, tend to shrink the optimal lamellar spacing. This behavior is qualitatively compatible with particle simulations that suggest that systems prepared by spray coating (corresponding to highly compressed initial single-chain configurations) form lamellae with a slightly larger spacing than systems that have been prepared by solvent casting.[44]

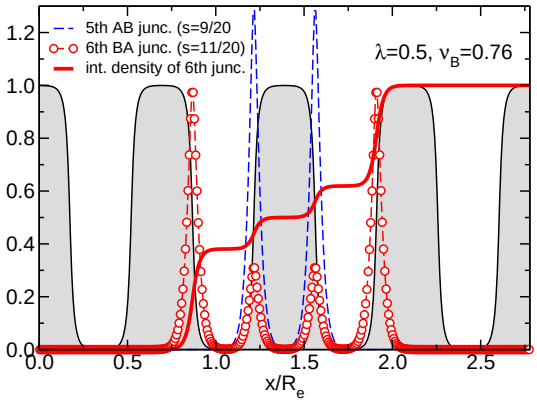

Figure 9: Illustration of calculation of the fraction of bridges of the middle B block of an 11-block copolymer ($M = 5$) at $\chi N = 400$, $\lambda = 0.5$, and $L = 0.6946 R_e$. The 5^{th} junction is constrained within the period between $1.0419 \leq x/R_e < 1.7365$

Using a system that is comprised of 4 lamellae, we calculate the fraction of loops and bridges. To illustrate the calculation, we focus on the B block between the 5^{th} and 6^{th} junction of an 11-block copolymer, $M = 5$. The probability that this block forms a loop is given by the conditional probability that the starting point of the B block, $\mathbf{r}(s = 9/20)$, is located in the unit cell V_A of thickness L centered around a specific A lamella, *i.e.*, $1.0419 \leq x/R_e < 1.7365$ in Figure 9, and that the end point of the B block, $\mathbf{r}(s = 11/20)$, is located in the same unit cell. Following Matsen and Thompson,[42] we define the conditional propagator

$$\bar{p}^L_{\boldsymbol{\eta}}(\mathbf{r}, s = 9/20) = \bar{p}_{\boldsymbol{\eta}}(\mathbf{r}, s = 9/20)\Theta_{V_A}(\mathbf{r}) \qquad \text{with} \quad \Theta_{V_A}(\mathbf{r}) = \begin{cases} 1 & \text{for} \quad \mathbf{r} \in V_A \\ 0 & \text{otherwise} \end{cases} \tag{115}$$

Using $\bar{p}^L_{\boldsymbol{\eta}}(\mathbf{r}, s = 9/20)$ as initial condition in Equation 41, we compute $\bar{p}^L_{\boldsymbol{\eta}}(\mathbf{r}, s)$ for $s > 9/20$, and obtain the density, $\phi^L(\mathbf{r}, s)$, of segments, $s > 9/20$, of 11-block copolymers whose 5$^{\text{th}}$ junction point is located in V_A. The density profiles for the 5$^{\text{th}}$ and 6$^{\text{th}}$ junction point are presented in Figure 9, as well as the integrated density $\int^x \mathrm{d}x'\, \phi^L(x', s = 11/20)$.

The loop probability for the B block between the 5$^{\text{th}}$ and 6$^{\text{th}}$ junction point is given by

$$1 - \nu_B = \frac{\int_{V_A} \mathrm{d}\mathbf{r}\, \bar{\phi}(\mathbf{r}, s = 11/20)}{\int_V \mathrm{d}\mathbf{r}\, \bar{\phi}(\mathbf{r}, s = 11/20)} \tag{116}$$

The results of this calculation for symmetric triblocks and 11-block copolymer are presented in

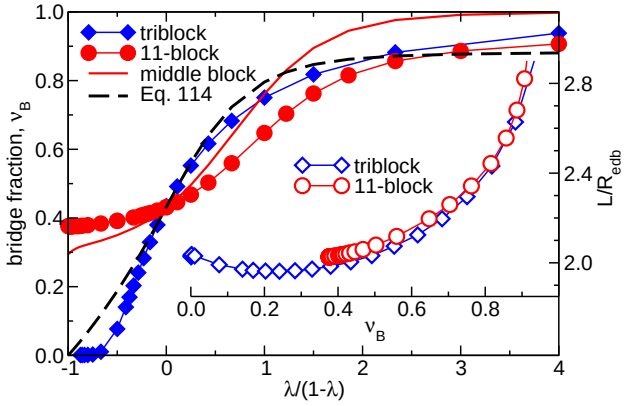

Figure 10: Bridge fraction, ν_{B}, of a symmetric 11-block copolymer ($M = 5$) at $\chi N = 400$, a symmetric triblock ($M = 1$) at $\chi N = 80$, and comparison to Equation 114 for the 11-block copolymer (dashed line). The solid line additionally shows the bridge fraction of the middle block of the 11-block copolymer. Inset: Lamellar spacing, L, in units of the end-to-end distance of the corresponding diblock copolymer as a function of the bridge fraction, ν_{B}.

Figure 10. As expected, the number of bridges increases as the chain extension increases with λ. Varying the strength of the orienting field, λ, we are able to tune the bridge fraction of the triblock copolymer over the entire range, $0 < \nu_{\mathrm{B}} < 1$. For the 11-block copolymer, chain stretching ($\lambda > 0$) remains quite effective in increasing the bridge fraction, however, the average bridge fraction cannot be reduced below 0.37 even for strongly compressed multiblock copolymers, $\lambda = -1000$ or $6\pi^2 \left(\mathbb{X}_1^2\right)_{xx} / R_{\mathrm{e}}^2 \approx 0.001$. Moreover, the middle block of the 11-block copolymer is more likely to bridge a lamellar domain than the average block if the multiblock is stretched, $\lambda > 0$, whereas it is more likely to form a loop in case of compression, $\lambda < 0$. Taken together, the control of the overall, large-scale chain conformations by constraining the variance of the first Rouse mode directly correlates with the bridge fraction of multiblocks that are comprised of few blocks and where each

block is a sizable fraction of the entire chain. In the limit of many blocks, $M \gg 1$, however, the properties of a block correspond to a small-scale property that correlates significantly less with $\mathbb{K}_1^2$. Accordingly, the simple prediction for copolymers with many blocks provides only a rough qualitative description for the bridge fraction of the 11-block copolymer. It tends to underestimate the number of bridges for small and large values of λ for the 11-block copolymer.

The inset of Figure 10 plots the optimal lamellar spacing, L, as a function of the bridge fraction, ν_B. Upon stretching the chains, $\lambda > 0$, both, ν_B and L, increase with λ – the more extended chains give rise to a larger lamellar spacing and to a higher fraction of bridges. Thus ν_B increases with the optimal spacing, L.[7]

For compressed ($\lambda < 0$ and ν_B small) triblock copolymers, however, we observe that the optimal spacing, L, decreases with an increasing number of bridges because the bridges add to the entropic penalty of chain stretching in the lamellar structure (see also insets of Figure 8). We hypothesize that this effect is not observed in our calculations for the 11-block copolymer because the control of $\mathbb{K}_1^2$ does not allow us to reduce the number of bridges sufficiently.

Conclusion and outlook

In summary, we have developed a SCFT for nongaussian molecular conformations that does not resort to the computationally expensive, partial enumeration over explicit chain conformations[59,61] but instead uses single-chain propagators that obey a modified diffusion equation, similar to SCFT for Gaussian chain molecules.[1–10] The constraint of the variance of the first Rouse mode gives rise to an additional integral over an auxiliary variable, $\boldsymbol{\eta}$, in the single-chain partition function. This integral cannot be evaluated by a saddlepoint approximation but can be treated efficiently by numerical discretization.

We have studied the behavior of symmetric, lamella-forming diblock and multiblock copolymers. Upon increasing the variance of the first Rouse mode, the diblock copolymers become more extended

[7] Note that this relation is just the opposite of what occurs upon expanding the lamellar spacing beyond its equilibrium value (for Gaussian chains, $\lambda = 0$), where the fraction of bridges decreases.

and "polarized". This results in a decrease of the incompatibility $\chi_{\mathrm{ODT}}N$ at the phase boundary between the disordered and lamellar phase and an increase of the optimal lamellar spacing, L. These effects are less pronounced for multiblock copolymers because the size of individual blocks is less affected by constraining the variance of the first Rouse mode. Instead the constraint on $\mathbb{X}_1^2$ controls the arrangement of blocks in space, which in turn impacts directly the fraction of bridges that the blocks form across the lamellar domains. Thus, by constraining the variance of the first Rouse mode we can describe systems with a nonequilibrium fraction of bridges. This situation is rather typical because the equilibration of the bridge fraction in strongly segregated lamellae is extremely slow.

Our approach has focused on constraining the variance of the first Rouse mode but the strategy can be generalized to quantities of the form $\hat{\mathbf{X}} \equiv \hat{\mathbf{r}}(s)f(s)$ with an arbitrary function, $f(s)$. This set of variables includes all the different Rouse modes as well as the end-to-end distance.[27]

In general, the variance of the first Rouse mode relaxes slowly towards its equilibrium value and therefore it will be important to study the kinetics of this slow, collective variable.[29] In a spatially homogeneous system of unentangled macromolecules, we expect the variance, $\mathbb{X}_1^2$, to decay exponentially in time according to the Rouse model.[45] Moreover, it would be interesting to derive a stress-composition coupling for inhomogeneous systems.[6,32,33]

As mentioned in the introduction, even steady flow will deform the molecular conformations, see Equation 2 for shear flow. The general form of the constitutive relation between incompressible, steady flow and molecular conformations in spatially homogeneous systems as well as specific expressions for unentangled chain molecules have been obtained by Ilg and Kröger[57] and are very useful to connect nonequilibrium conformations to the forces that drive the system out of equilibrium.

Acknowledgement

We acknowledge Q. Tang and J. Tang for stimulating discussions in the early stages of the project,

and thank K. Ch. Daoulas for critical reading of the manuscript. Financial support by the Deutsche Forschungsgemeinschaft (DFG) under grant Mu1674/15-2 is gratefully acknowledged. We thank the von Neumann Institute for Computing (NIC) for access to the supercomputer JUWELS at Jülich Supercomputing Centre (JSC). Additional computational resources at the HLRN Berlin/Göttingen were made available to the project.

References

(1) Helfand, E.; Tagami, Y. Theory of Interface between Immiscible Polymers. J. Polym. Sci. B: Polymer Letters **1971**, 9, 741.

(2) Scheutjens, J. M. H. M.; Fleer, G. J. Statistical-Theory of the Adsorption of Interacting Chain Molecules .1. Partition-Function, Segment Density Distribution, and Adsorption-Isotherms. J. Phys. Chem. **1979**, 83, 1619–1635.

(3) Hong, K. M.; Noolandi, J. Theory of Inhomogeneous Multicomponent Polymer Systems. Macromolecules **1981**, 14, 727–736.

(4) Matsen, M. W.; Schick, M. Stable and unstable phases of a diblock copolymer melt. Phys. Rev. Lett. **1994**, 72, 2660–2663.

(5) Shi, A. C.; Noolandi, J.; Desai, R. C. Theory of Anisotropic Fluctuations in Ordered Block Copolymer Phases. Macromolecules **1996**, 29, 6487–6504.

(6) Fredrickson, G. H. Dynamics and Rheology of Inhomogeneous Polymeric Fluids: a Complex Langevin Approach. J. Chem. Phys. **2002**, 117, 6810–6820.

(7) Fredrickson, G. H. The equilibrium theory of inhomogeneous polymers; Clarendon press: Oxford, 2006.

(8) Müller, M.; Schmid, F. Incorporating fluctuations and dynamics in self-consistent field theories for polymer blends. Adv. Polym. Sci **2005**, 185, 1–58.

(9) Tyler, C. A.; Morse, D. C. Orthorhombic *Fddd* Network in Triblock and Diblock Copolymer Melts. Phys. Rev. Lett. **2005**, 94, 208302.

(10) Shi, A.-C.; Li, B. Self-assembly of diblock copolymers under confinement. Soft Matter **2013**, 9, 1398–1413.

(11) Altevogt, P.; Evers, O. A.; Fraaije, J. G. E. M.; Maurits, N. M.; van Vlimmeren, B. A. C. The MesoDyn project: software for mesoscale chemical engineering. J. Mol. Struct. THEOCHEM **1999**, 463, 139–143.

(12) Maurits, N. M.; Fraaije, J. G. E. M. Mesoscopic Dynamics of Copolymer Melts: from Density Dynamics To External Potential Dynamics Using Nonlocal Kinetic Coupling. J. Chem. Phys. **1997**, 107, 5879–5889.

(13) Reister, E.; Müller, M.; Binder, K. Spinodal Decomposition in a Binary Polymer Mixture: Dynamic Self-Consistent-Field Theory and Monte Carlo Simulations. Phys. Rev. E **2001**, 64, 041804.

(14) Morita, H.; Kawakatsu, T.; Doi, M. Dynamic Density Functional Study on the Structure of Thin Polymer Blend Films with a Free Surface. Macromolecules **2001**, 34, 8777–8783.

(15) Honda, T.; Kawakatsu, T. Hybrid Dynamic Density Functional Theory for Polymer Melts and Blends. Macromolecules **2007**, 40, 1227–1237.

(16) Cheng, X. Y.; Lin, L.; E, W.; Zhang, P. W.; Shi, A. C. Nucleation of Ordered Phases in Block Copolymers. Phys. Rev. Lett. **2010**, 104, 148301.

(17) Takahashi, H.; Laachi, N.; Delaney, K. T.; Hur, S.-M.; Weinheimer, C. J.; Shykind, D.; Fredrickson, G. H. Defectivity in Laterally Confined Lamella-Forming Diblock Copolymers: Thermodynamic and Kinetic Aspects. Macromolecules **2012**, 45, 6253–6265.

(18) Li, W. H.; Nealey, P. F.; de Pablo, J. J.; Müller, M. Defect removal in the course of directed

self-assembly is facilitated in the vicinity of the order-disorder transition. Phys. Rev. Lett. **2014**, 113, 168301.

(19) Kawasaki, K.; Sekimoto, K. Concentration dynamics in polymer blends and block copolymer melts. Macromolecules **1989**, 22, 3063–3075.

(20) Abetz, V.; Kremer, K.; Müller, M.; Reiter, G. Functional Macromolecular Systems: Kinetic Pathways to Obtain Tailored Structures. Macromol. Chem. Phys. **2019**, 220, 1800334, DOI: 10.1002/macp.201800334.

(21) Chandran, S.; Baschnagel, J.; Cangialosi, D.; Fukao, K.; Glynos, E.; Janssen, L. M. C.; Müller, M.; Muthukumar, M.; Steiner, U.; Xu, J.; Napolitano, S.; Reiter, G. Processing Pathways Decide Polymer Properties at the Molecular Level. Macromolecules **2019**, 52, 7146–7156, DOI: 10.1021/acs.macromol.9b01195.

(22) Reiter, G. The memorizing capacity of polymers. J. Chem. Phys. **2020**, 152, 150901, DOI: 10.1063/1.5139621.

(23) Wang, G.; Ren, Y.; Müller, M. Collective Short-Time Dynamics in Multicomponent Polymer Melts. Macromolecules **2019**, 52, 7704–7720.

(24) Müller, M.; Sun, D. W. Directing the Self-Assembly of Block Copolymers into A Metastable Complex Network Phase via A Deep and Rapid Quench. Phys. Rev. Lett. **2013**, 111, 267801.

(25) Müller, M. Process-directed self-assembly of copolymers: Results of and challenges for simulation studies. Prog. Polym. Sci. **2020**, 101, 101198.

(26) Bruns, W.; Carl, W. Chain Extension in Steady Shear-Flow. Macromolecules **1993**, 26, 557–558.

(27) Mavrantzas, V. G.; Theodorou, D. N. Atomistic Simulation of Polymer Melt Elasticity: Calculation of the Free Energy of an Oriented Polymer Melt. Macromolecules **1998**, 31, 6310–6332.

(28) Wang, X.; Chatterjee, A. P. Chain Orientation and Extension in Steady Shear Flow. Macromolecules **2001**, 34, 1118–1121.

(29) Baig, C.; Mavrantzas, V. G. Multiscale simulation of polymer melt viscoelasticity: Expanded-ensemble Monte Carlo coupled with atomistic nonequilibrium molecular dynamics. Phys. Rev. B **2009**, 79, 144302.

(30) Ilg, P.; Öttinger, H.; Kröger, M. Systematic time-scale-bridging molecular dynamics applied to flowing polymer melts. Phys. Rev. E **2009**, 79, 011802.

(31) Baig, C.; Mavrantzas, V. G.; Kröger, M. Flow Effects on Melt Structure and Entanglement Network of Linear Polymers: Results from a Nonequilibrium Molecular Dynamics Simulation Study of a Polyethylene Melt in Steady Shear. Macromolecules **2010**, 43, 6886–6902.

(32) Helfand, E.; Fredrickson, G. H. Large fluctuations in polymer solutions under shear. Phys. Rev. Lett. **1989**, 62, 2468–2471.

(33) Doi, M.; Onuki, A. Dynamic coupling between stress and composition in polymer solutions and blends. J. Phys. II **1992**, 2, 1631–1656.

(34) Pryamitsyn, V.; Ganesan, V. Correlations in Block Copolymers Under Shear. Macromolecules **2002**, 35, 9847–9850.

(35) Fraser, B.; Denniston, C.; Müser, M. H. On the orientation of lamellar block copolymer phases under shear. J. Chem. Phys. **2006**, 124, 104902.

(36) Peters, B. L.; Ramirez-Hernandez, A.; Pike, D. Q.; Müller, M.; de Pablo, J. J. Nonequilibrium Simulations of Lamellae Forming Block Copolymers under Steady Shear: A Comparison of Dissipative Particle Dynamics and Brownian Dynamics. Macromolecules **2012**, 45, 8109–8116, DOI: 10.1021/ma301541f.

(37) Shagolsem, L. S.; Kreer, T.; Sommer, J.-U. Shear-Induced Ordering in Thin Films of Diblock Copolymer Melts. ACS Macro Letters **2014**, 3, 1201–1204.

(38) Schneider, L.; Heck, M.; Wilhelm, M.; Müller, M. Transitions between Lamellar Orientations in Shear Flow. Macromolecules **2018**, 51, 4642–4659.

(39) Schneider, L.; Müller, M. Rheology of symmetric diblock copolymers. Comput. Mater. Sci. **2019**, 169, 109107.

(40) Matsen, M. W. Bridging and looping in multiblock copolymer melts. J. Chem. Phys. **1995**, 102, 3884.

(41) Rasmussen, K. Ø.; Kober, E. M.; Lookman, T.; Saxena, A. Morphology and bridging properties of $(AB)_n$ multiblock copolymers. J. Polym. Sci. B: Polym. Phys. **2003**, 41, 104–111.

(42) Matsen, M. W.; Thompson, R. B. Equilibrium behavior of symmetric ABA triblock copolymer melts. J. Chem. Phys. **1999**, 111, 7139–7146.

(43) Drolet, F.; Fredrickson, G. H. Optimizing Chain Bridging in Complex Block Copolymers. Macromolecules **2001**, 34, 5317–5324.

(44) Tang, Q.; Tang, J.; Müller, M. Process-directed self-assembly of multiblock copolymers: Solvent casting vs spray coating. Eur. Phys. J. Spec. Top. **2016**, 225, 1785–1803.

(45) Rouse, P. E. A Theory of the Linear Viscoelastic Properties of Dilute Solutions of Coiling Polymers. J. Chem. Phys. **1953**, 21, 1272–1280.

(46) Doi, M.; Edwards, S. F. The Theory of Polymer Dynamics, Clarendon Press, Oxford **1986**,

(47) Mavrantzas, V. G.; Öttinger, H. C. Atomistic Monte Carlo Simulations of Polymer Melt Elasticity: Their Nonequilibrium Thermodynamics GENERIC Formulation in a Generalized Canonical Ensemble. Macromolecules **2002**, 35, 960–975.

(48) Tzeremes, G.; Rasmussen, K.; Lookman, T.; Saxena, A. Efficient computation of the structural phase behavior of block copolymers. Phys. Rev. E **2002**, 65, 041806.

(49) Rasmussen, K.; Kalosakas, G. Improved numerical algorithm for exploring block copolymer mesophases. J. Polym. Sci. B: Polym. Phys. **2002**, 40, 1777–1783.

(50) Holyst, R.; Schick, M. Correlations in a rigid–flexible diblock copolymer system. J. Chem. Phys. **1992**, 96, 730–739.

(51) Hamm, M.; Goldbeck-Wood, G.; Zvelindovsky, A. V.; Sevink, G. J. A.; Fraaije, J. G. E. M. Structure formation in liquid crystalline polymers. J. Chem. Phys. **2002**, 116, 3152–3161.

(52) Daoulas, K. C.; Rühle, V.; Kremer, K. Simulations of nematic homopolymer melts using particle-based models with interactions expressed through collective variables. J. Phys.: Condens. Matter **2012**, 24, 284121.

(53) Cai, Y.; Zhang, P.; Shi, A.-C. Liquid crystalline bilayers self-assembled from rod–coil diblock copolymers. Soft Matter **2017**, 13, 4607–4615.

(54) Jiang, Y.; Greco, C.; Daoulas, K. Ch.; Chen, J. Z. Y. Thermodynamics of a Compressible Maier-Saupe Model Based on the Self-Consistent Field Theory of Wormlike Polymer. Polymers **2017**, 9, 48.

(55) Sarti, G. C.; Marrucci, G. Thermomechanics of dilute polymer solutions: multiple bead-spring model. Chem. Eng. Sci. **1973**, 28, 1053–1059, DOI: 10.1016/0009-2509(73)80008-9.

(56) Booij, H. C. The energy storage in the Rouse model in an arbitrary flow field. J. Chem. Phys. **1984**, 80, 4571–4572, DOI: 10.1063/1.447210.

(57) Ilg, P.; Kröger, M. Molecularly derived constitutive equation for low-molecular polymer melts from thermodynamically guided simulation. J. Rheol. **2010**, 55, 69, DOI: 10.1122/1.3523485.

(58) Leibler, L. Theory of Microphase Separation in Block Co-Polymers. Macromolecules **1980**, 13, 1602–1617.

(59) Müller, M.; Tang, J. Alignment of copolymer morphology by planar step elongation during spinodal self-assembly. Phys. Rev. Lett. **2015**, 115, 228301.

(60) Pincus, P. Excluded Volume Effects and Stretched Polymer Chains. Macromolecules **1976**, 9, 386–388.

(61) Szleifer, I.; Carignano, M. A. Tethered Polymer Layers. Adv. Chem. Phys. **1996**, 94, 165–260.

Graphical TOC Entry

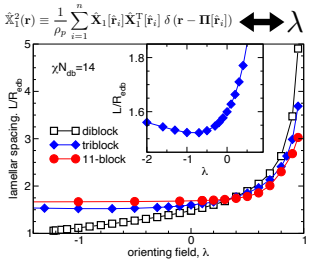

Periodicity of multi-blocks:
Compression of tri-block configurations increases periodicity